Thesis

Evaluation of the hypointense rim sign on susceptibility weighted imaging in treated glioblastoma

submitted by

Jakob Witsch

in partial fulfilment of the requirements for the degree of

Doktor der gesamten Heilkunde
(Dr. med. univ.)

at the

Medical University of Graz

executed at the

Division of Neuroradiology
Department of Radiology

under the supervision of

Ao. Univ.-Prof. Dipl.-Ing. Dr.med.univ. Josef Simbrunner, PhD
and
Dr.med.univ. Marton Magyar

Graz, 10.09.2025

Declaration of Academic Integrity

I hereby confirm that the present diploma thesis is the result of my own independent scholarly work. I also confirm that in all cases, where material from the work of others (in books, articles, essays, dissertations, and on the internet) is acknowledged, quotations and paraphrases are clearly indicated. No material other than that cited in the reference list has been used. I have read and understood the Medical University's regulations and procedures concerning plagiarism.

Furthermore, I hereby declare that if artificial intelligence (AI) tools were used for the generation and/or correction of certain text passages in the creation of this work, such employment was conducted in compliance with ethical principles, academic integrity, and the regulations of my university. Additionally, it was ensured that this usage was transparently disclosed and appropriately attributed.

Graz, 21.07.2025 *Jakob Witsch, m.p.*

Acknowledgements

I would like to thank all those who supported me on this journey.

First, I would like to express my sincere gratitude to Prof. Dr. Deutschmann for the opportunity to complete my diploma thesis at the Department of Neuroradiology.
My deepest thanks go to Prof. Dr. Simbrunner and Dr. Marton Magyar, who consistently supported me throughout this project. I am especially grateful to Dr. Magyar for the many evenings he dedicated to analyzing the imaging data with me.

I am forever grateful to my family, who have supported me unconditionally since the very beginning of my medical education.
I am particularly thankful to my parents, grandparents, and siblings for their continuous interest in my work and their unwavering belief in me.

Finally, I would like to thank my girlfriend, Dana, who stood by my side, especially during the challenging moments, and never stopped trying to keep me positive.

Zusammenfassung

Hintergrund: Das Glioblastom (GBM) ist ein aggressiver, primärer Hirntumor mit schlechter Prognose. Die Beurteilung des Therapieansprechens und der Krankheitsprogression ist trotz der Einführung der RANO-Kriterien eine Herausforderung. Suszeptibilitätsgewichtete Bildgebung (SWI) hat sich als wertvolle MRT-Sequenz zur Darstellung neuropathologischer Prozesse etabliert und ist besonders sensitiv für Blutabbauprodukte und Eisenablagerungen. Bei der Multiplen Sklerose (MS) konnte gezeigt werden, dass ein hypointenser Randsaum von Plaques in suszeptibilitätsgewichteten Bildern mit einem schwereren Krankheitsverlauf assoziiert ist. Beim Glioblastom wurde eine prognostische Bedeutung eines solchen Randsaumes noch nicht untersucht.

Ziel: Diese Studie hatte das Ziel, Prävalenz, Morphologie und die prognostische Relevanz des hypointensen Randsaumes in der SWI bei Patient:innen mit Glioblastom zu untersuchen.

Methodik: In diese Studie wurden retrospektiv Patient*innen mit histologisch gesichertem IDH-wildtype-Glioblastom, welche eine Standardtherapie erhalten haben eingeschlossen. Für jede Person wurde das erste post-radiotherapeutische MRT mit einem Tumor >10 mm analysiert. Falls verfügbar, wurden auch präoperative MRTs ausgewertet. Der Randsaum wurde als lineare Signalabschwächung am Rand des kontrastmittelanreichernden Tumors definiert und auf Vollständigkeit und Kontur hin bewertet. Im Anschluss erfolgte eine Korrelationsanalyse mit weiteren bildgebenden Merkmalen sowie eine Überlebensanalyse mittels Cox-Regression.

Ergebnisse: Insgesamt wurden 55 Patient*innen (Durchschnittsalter 59,5 ± 10,9 Jahre; 29 Männer, 26 Frauen) in die Analyse eingeschlossen. Ein hypointenser Randsaum war in 37 von 55 post-radiotherapeutischen MRTs (67,3%) nachweisbar. In einer Subanalyse von 19 Patient:innen mit prä- und post-radiotherapeutischem MRT stieg die Prävalenz eines Rims mit glattem Rand signifikant an ($p = 0{,}003$). Der Rim war signifikant mit dem Muster der Kontrastmittelanreicherung assoziiert ($p = 0{,}004$) und fehlte bei allen Tumoren mit netzartiger Kontrastmittelaufnahme. Es zeigten sich keine signifikanten Assoziationen mit anderen erhobenen Parametern. Ein glatter Randsaum war signifikant mit einem längeren Gesamtüberleben assoziiert ($HR = 0{,}47$; $p = 0{,}018$) und stellte auch in der multivariaten Analyse einen unabhängigen prognostischen Faktor dar.

Diskussion: Unsere Analyse zeigte, dass ein hypointenser Randsaum bei einem beträchtlichen Anteil von Patient*innen mit Glioblastom vorkommt und in Übereinstimmung mit den Beobachtungen anderer Studien morphologisch als glatt oder unregelmäßig klassifiziert werden kann. Glatte Rims traten häufiger nach der Radiotherapie auf und waren signifikant mit einem län-

geren Überleben assoziiert. Das legt nahe, dass der Rim behandlungsinduzierte Veränderungen des Tumormikromilieus widerspiegeln könnte, die möglicherweise Aufschluss über das Therapieansprechen und die Tumorprogression geben. Zukünftige Studien sollten diese Ergebnisse in größeren, prospektiven Kohorten validieren und radiopathologische Korrelationen einbeziehen.

Abstract

Background: Glioblastoma (GBM) is a highly aggressive primary brain tumor with bad prognosis. Assessing treatment response and disease progression remains challenging, despite the introduction of RANO-criteria. Susceptibility-weighted imaging (SWI) has emerged as a valuable MRI sequence for characterizing neuropathological processes, and is particularly sensitive to hemorrhage, calcification, or iron deposition. While a hypointense rim sign on SWI has been described in multiple sclerosis and is associated with a more severe disease burden, its prognostic role in glioblastoma remains unexplored.

Objective: This study evaluates the presence, morphology, and prognostic relevance of the hypointense rim sign on SWI in patients with glioblastoma.

Methods: We retrospectively included patients with histologically confirmed IDH-wildtype glioblastoma who underwent standard therapy. For each patient, the first post-radiotherapy MRI scan demonstrating a contrast-enhancing tumor >10 mm was selected for analysis. If available, pre-surgery MRI scans were also reviewed. The hypointense rim sign was defined as a linear signal hypointensity located in the periphery of the contrast-enhancing tumor. Rims were assessed for completeness and contour, and correlated with additional imaging features. Cox regression analysis was used for survival analysis.

Results: A total of 55 patients (mean age 59.5 ± 10.9 years; 29 males, 26 females) were included in the final analysis. A hypointense rim on SWI was present in 37 out of 55 post-radiotherapy MRIs (67.3%). In the paired subanalysis of 19 patients with both pre- and post-radiotherapy MRI, the prevalence of smooth rims increased significantly from 5.3% pre-surgery to 63.2% post-radiotherapy ($p = 0.003$). The presence of a hypointense rim on post-radiotherapy scans was significantly associated with contrast enhancement pattern ($p = 0.004$), being absent in all tumors with net-like enhancement. No significant associations were found with other clinical or imaging parameters. A smooth rim was significantly associated with longer overall survival (HR = 0.47; $p = 0.018$), and remained an independent prognostic factor in multivariate analysis.

Discussion: Our analysis showed that a hypointense rim is present in a substantial proportion of glioblastoma patients and, consistent with previous studies, can be categorized as either smooth or irregular. Smooth rims were more common after radiotherapy and significantly associated with longer overall survival. This suggests, that the rim potentially represents microenvironmental changes that could provide information on treatment response and tumor progression. Future studies should aim to validate these findings in larger, prospective cohorts and include radiopathological correlation.

Table of Contents

I. Abbreviations

ADC	apparent diffusion coefficient
BBB	blood-brain-barrier
CCNU	lomustine
C-index	concordance index
CI	confidence intervals
CNS	central nervous system
CSF	cerebrospinal fluid
DWI	diffusion-weighted imaging
EOR	extent of tumor resection
FDA	US Food and Drug Administration
FLAIR	fluid-attenuated inversion recovery
FOV	field of view
GBM	glioblastoma
GFAP	glial fibrillary acidic protein
HR	hazard ratios
IDH	isocitrate dehydrogenase
ITSS	Intratumoral susceptibility signals
MS	multiple sclerosis
NCCN	National Comprehensive Cancer Network
NCI	National Cancer Institute
OS	overall survival
PFS	progression-free survival
PRL	paramagnetic rim lesion
PTE	peritumoral edema
PsP	pseudoprogression
PWI	perfusion weighted imaging
RANO	Response Assessment in Neuro-Oncology

RCTs	randomized controlled trials
rCBV	relative cerebral blood volume
RF	radiofrequency
RN	radiation necrosis
SusE	susceptibility effects
T1-wi	T1-weighted imaging
TE	echo time
TI	inversion time
TMZ	temozolomide
TR	repetition time
TAMs	Tumor associated macrophages
WHO	World health organization
VEGF	vascular endothelial growth factor

II. List of Figures

III. List of Tables

1 Introduction

1.1 Adult type diffuse gliomas

1.1.1 Definition

The term ”glioma” is used to describe a neuroepithelial tumor that originates from glial cells of the central nervous system (CNS). Glial cells are the most prevalent cell type in the CNS and have the function of isolating neurons as well as supplying them with oxygen and nutrients. Gliomas account for 24% of all primary CNS tumors, making them the second most prevalent group after meningiomas. As gliomas vary significantly, both histologically and in terms of clinical outcome, a good classification system had to be established [1].

1.1.2 Classification

Historically, the classification of CNS-tumors was primarily based on histological findings, where tumors were categorized according to their appearance under a microscope. This approach, known as histogenetic classification, relied heavily on the tumor’s structure and cellular morphology to determine its type and grade. However, in the past decade , research has shown that it is much more effective to characterize tumor entities based on a molecular assessment. This shift from a purely histological to a molecular approach is largely due to the discovery that tumors with similar histological features can have very different genetic and molecular characteristics, which affects their behavior, prognosis and response to treatment. The World Health Organization (WHO) started to incorporate molecular criteria for classification in 2016 [1].

In the most recently published CNS-5 classification system from 2021 this approach is taken further by grouping together tumors not on their appearance but mainly on their molecular patterns. It is for this reason, that in the WHO CNS-5 classification gliomas are still recognized as a major category, but they are now integrated into a broader classification that includes glioneuronal and neuronal tumors. The classification system reorganized gliomas, glioneuronal tumors, and neuronal tumors into the following six different families: adult-type diffuse gliomas, pediatric-type low-grade and high-grade diffuse gliomas, glioneuronal and neuronal tumors, circumscribed astrocytic gliomas and ependymal tumors [2].

Tumor Grading

Another important thing that changed with the WHO CNS-5 classification is the grading of gliomas. Before 2021, tumor grading could be applied across tumor types, which meant that tumors of different origin and with different molecular patterns were compared on a common scale. For example, a grade III meningioma and a grade III astrocytoma were expected to

have similar survival times, but this approach was often inaccurate. The CNS-5 classification introduced tumor grading within specific types, which is better suited to reflect the biological behavior and clinical outcomes. Arabic numerals are used instead of roman numerals, as this is also the more common approach in other tumor types. In addition to this shift to tumor grading within specific types there was also a shift from histopathological grading towards molecularpathological grading. The grade is still mainly assigned with respect to cellularity, mitotic, activity, necrosis but molecularpathological markers gained influence. Some genetic markers associated with poor prognosis can now result in a tumor being assigned a grade of 4, independent of the histopathological findings [2].

The group of adult-type diffuse gliomas includes three main tumor types: IDH-mutant astrocytomas, IDH-mutant and 1p/19q-codeleted oligodendrogliomas, as well as IDH-wildtype glioblastomas. These entities that are grouped together because they share important molecular pathways, particularly those involving the isocitrate dehydrogenase (IDH) gene.

IDH

The two IDH-enzymes, act as catalysts in the oxidative decarboxylation of isocitrate, which produces alpha-ketoglutarate and carbon dioxide. This reaction plays a significant role in cellular metabolism. IDH-1 and IDH-2, are highly similar in their biochemical properties, however, there are differences in their cellular localization. IDH-1 is mainly found in the cytoplasm, while IDH-2 is primarily located in the mitochondria. In the mutated state, IDH1 and IDH2 enzymes gain a new function, catalyzing the conversion of α-ketoglutarate into 2-hydroxyglutarate (2-HG). The production of 2-HG is associated with alterations in cellular metabolism and epigenetics, which appears to impact the growth and progression of these tumors. Patients with IDH-mutant gliomas typically show a significantly longer survival compared to those with wildtype IDH. Consequently, there is ongoing research to gain a deeper understanding of the role of IDH1 and IDH2 in glioma, with the goal to develop more effective molecular therapies. [3]

Astrocytoma, IDH-mutant

Astrocytic tumors consist of cells characterized by elongated or irregular hyperchromatic nuclei and cytoplasm that is eosinophilic and positive for glial fibrillary acidic protein (GFAP). This tumor type is defined by the presence of an IDH1 or IDH2 mutation in a diffuse glioma, together with an ATRX-mutation or absence of 1p19q codeletion [4]. Typically, the tumor grade is assigned depending on the histological findings, however if there is CDKN2A/B-deletion, grade 4 is assigned due to bad prognosis regardless of other morphological features. Grade 4 IDH-mutated astrocytomas were previously called IDH-mutated glioblastomas, and as mentioned show a better prognosis than the glioblastoma, IDH-wildtype [5].

Oligodendroglioma, IDH-mutant and 1p/19q-codeleted

In contrast to astrocytic tumors, oligodendrogliomas are identified by their rounded nuclei, often surrounded by perinuclear halos, and are associated with calcification and delicate, branching blood vessels. These tumors are characterized by the presence of IDH1/2 mutations and the codeletion of chromosomal arms 1p and 19q [5].

Glioblastoma (GBM), IDH-wildtype

Glioblastoma (GBM), IDH-wildtype, is the most common malignant primary brain tumor in adults [6]. These tumors are highly cellular, pleomorphic, and exhibit diffuse infiltration along with high mitotic activity. Its diagnosis requires the absence of IDH mutations and the presence of another key molecular or histopathological feature, which are shown in Figure 1 [7].

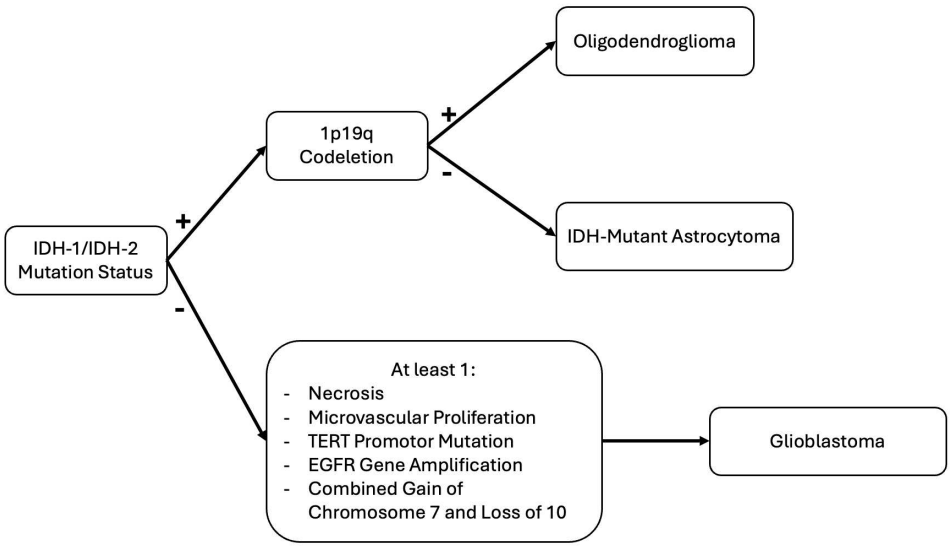

Figure 1: Diagnostic classification of adult-type diffuse gliomas. Schematic overview of the diagnostic pathway based on the 2021 WHO Classification of Tumors of the Central Nervous System. Adapted from Vagvala et al. [7].

1.1.3 Clinical features

The symptoms of brain tumors can vary greatly, primarily depending on the tumor's location and pathology. Typically, symptoms are focal initially and progress to generalized symptoms as the tumor expands. Symptoms associated with high-grade tumors typically progress more rapidly than those of low-grade tumors [8].

Focal deficits

When the tumor is located in a critical region of the brain, focal symptoms, which are specific to the function of the region, may occur. Lesions near or in the motor cortex may cause paresis, which is characterized by muscle weakness or partial loss of movement. Characteristic for this type of paresis is partial reversibility through the administration of glucocorticoids, which help to reduce edema and therefore the mass effect of the tumor [9].
Besides paresis other symptoms like sensory deficits, aphasia and visual dysfunction may also occur. Since gliomas can occur in any part of the central nervous system, a wide range of associated symptoms is possible [8].

Headache

In more than half of the patients, headache is the presenting symptom of brain tumors, but specify is low. Since brain tissue itself lacks sensory innervation, pain is caused by direct pressure on structures within the brain that do have sensory innervation such as arteries, cranial nerves or cerebral meninges. Most commonly headache presents 'tension-like', constant and worsens when changing body position. Even though headache is a frequent symptom in brain tumors, isolated headache as an initial manifestation is uncommon, more often it is accompanied by other neurological symptoms [10].

Seizures

Seizures are another frequent symptom of brain tumors, occurring in approximately 75% of IDH-mutated grade 2 astrocytomas and around 25% of wild-type glioblastomas. Seizures are more typically in low-grade gliomas as the mutation in the IDH-enzymes leads to the production of 2-hydroxyglutarate which is similar to glutamate - an excitatory neurotransmitter [11, 12].
Seizures are defined as "a transient occurrence of signs and/or symptoms due to abnormal excessive or synchronous neuronal activity in the brain" [13]. In brain tumors, seizures are primarily caused by structural damage to brain tissue due to tumor infiltration, as well as changes in pH and ion levels in the peritumoral brain tissue. The specific clinical manifestation of a seizure is mainly related to the tumors' location in the brain. Tumors in the frontal lobe may cause focal tonic-clonic movements that are restricted to one arm. In contrast, tumors in the occipital lobe typically lead to visual disturbances like hallucinations or visual field defects [14].

Neurocognitive dysfunction

Another common symptom of brain tumors is neurocognitive dysfunction, which occurs in more than 90% of patients with supratentorial brain tumors over the course of the disease.

This dysfunction can be attributed to various factors, including tissue damage from necrosis, compression of neural structures due to the tumor's mass effect, and the infiltration of critical neural fiber pathways. Patients often show deficits in various neurocognitive functions, including language processing, memory and executive function. Problems with disinhibited behavior, such as increased aggression and impulsivity are particulary challanging for those around the patient. Surgical resection of the tumor can lead to an improvement in symptoms, as it may reduce pressure on surrounding brain tissue [15].

1.1.4 Treatment approaches

Before the discovery of important molecular markers, therapy for diffuse gliomas was mainly based on histologic subtype and tumor grade. However, the increased significance of markers like IDH and 1p/19q, which allow the differentiation of mutant astrocytomas, oligodendrogliomas, and glioblastomas, has led to a more specific therapeutic approach. Despite differences in biological behavior and aggressiveness, all diffuse gliomas can be considered incurable due to their high rate of recurrence [16].

Surgical management

Initial maximal surgical resection is considered the preferred first line approach for all types of diffuse glioma. The extent of surgical intervention varies based on the tumor's location and growth pattern. If there is a risk to damage critical brain regions, minimally invasive biopsy may be performed. However, if safe resection is possible, craniotomy with the goal of complete tumor mass removal is preferred. To minimize the risk of iatrogenic neurological deficits while maximizing resection, advanced tools such as surgical navigation systems incorporating functional MRI, diffusion tensor imaging, intraoperative MRI, and fluorescence-based tumor visualization are used [17].

The extent of tumor resection (EOR) is important for prognostic evaluations and should be investigated 24 to 48 h after surgery by using MRI with and without contrast. While EOR was traditionally evaluated by the neurosurgeon, it is now well established that post-surgical MRI assessments performed by neuroradiologists are much more sensitive. The time-window of post-surgical MRI is important, as surgical intervention cause reactive changes that can be misinterpreted as residual tumor growth. Especially between post-operative days 4 and 21, MRI scans often show marginal 'reactive' enhancement, which is caused by hypervascularization and blood-brain barrier disruptions resulting from the surgical procedure rather than residual tumor [18].

It is important to note, that even though increased residual tumor volume after surgery is associated with worse outcomes in gliomas of all grades, minimizing neurological deficits caused

by surgery remains the primary priority. Additional surgery-induced neurological deficits not only have a severe impact on the patients' quality of life, but also might add additional complications which do not allow further therapy which is essential in glioma patients [17].

Radiochemotherapy

After surgery, adjuvant treatment, such as radiotherapy and chemotherapy, is necessary in most cases of diffuse gliomas. Newly diagnosed IDH-mutated grade 2 gliomas have several options available after treatment, including watchful waiting, radiotherapy (RT) plus chemotherapy and IDH-targeted therapy. However, in diffuse gliomas of a WHO grade 3 or higher, an immediate postoperative RT in combination with adjuvant or concurrent chemotherapy is indicated [19].
As initial chemotherapeutic agent Temozolomide (TMZ), an oral DNA alkylating agent, is most commonly used. In grade 3 IDH-mutant astrocytomas, adjuvant therapy with TMZ following radiotherapy has been shown to significantly improve overall survival (OS) compared to no adjuvant TMZ treatment, as demonstrated in the CATNON trial. No benefit was seen with the concurrent treatment with TMZ [20].

For grade 3 oligodendrogliomas, which are characterized by the presence of a 1p/19q co-deletion, both TMZ and PCV (a combination of procarbazine, lomustine, and vincristine) are reasonable options for adjuvant therapy. The RTOG 9802 trial showed that PCV provides a survival benefit in patients with oligodendrogliomas. Another study, named CODEL, is currently evaluating PCV against TMZ in 1p/19q-codeleted tumors [17].

For grade 4 diffuse gliomas, which can be either IDH-mutated or IDH-wildtype (e.g. glioblastoma) RT plus concurrent TMZ followed by adjuvant TMZ is considered best treatment [19]. The standard treatment protocol for glioblastomas following surgical resection is the Stupp protocol, which includes radiotherapy to the postoperative tumor bed over six weeks (2 Gy per fraction, five days per week, totaling 60 Gy), combined with daily temozolomide at 75 mg/m² of body surface area, at seven days a week during RT. This is followed by six cycles of adjuvant TMZ, starting with 150 mg/m² daily for five days in a 28-day cycle, and escalating to 200 mg/m² if tolerated [18].

Second line treatment

Despite maximal safe resection and the use of adjuvant radiation- and chemotherapy most patients experience a relapse after the initial treatment. Consequently, follow-up MRI scans are recommended in treated gliomas with an initial interval of 2 to 6 months between scans

depending on tumor subtype and grade. The accurate interpretation and detection of progression in follow-up MRI scans will be explored in detail later in this work.

At recurrence, second-line treatment is highly influenced by the response to first-line therapy and treatment decisions must be individualized as there are no studies comparing active interventions versus best supportive care. Second surgery can be considered for all patients experiencing a relapse at least 6 months after the initial surgery, particularly those who are symptomatic, as debulking can help reduce symptomatic mass effect [17].

Re-irradiation is another treatment approach, however, there is no data from randomized controlled trials (RCTs) to investigate its efficacy in improving OS. Identifying patients who are most likely to benefit from re-irradiation therapy remains one of the major challenges [21].

For systematic therapy the most commonly used agents are bevacizumab, nitrosoureas, and temozolomide rechallenge. Bevacizumab is a monoclonal antibody that binds to circulating vascular endothelial growth factor (VEGF) and has shown a significant effect on MRI-features of gliomas [22]. However, in studies exploring the effect of bevacizumab on OS, no benefit was detected, and while being approved for the treatment of recurrent glioblastoma in the United States it is not approved in the European Union. The rechallenge with bevacizumab, as well as therapy with lomustine (CCNU), have both reported a similar 6-month progression free survival (PFS) of approximately 20%, but neither has demonstrated an improvement in overall survival. Despite this, CCNU is considered the most appropriate treatment option for patients with recurrent gliomas. [17].

1.2 MRI evaluation of gliomas

1.2.1 Initial evaluation

When patients present with the discussed neurological symptoms and there is a suspicion of a brain tumor, gadolinium-enhanced MRI is the preferred diagnostic method. Often a CT-scan is performed as initial neuroimaging tool and even though it provides important information on size and location of a mass-effect, MRI is superior for tumor characterization. Because of its high soft-tissue contrast and spatial resolution, MRI allows the detailed assessment of mass effect, edema, hemorrhage, necrosis, and indicators of elevated intracranial pressure, making it the current standard tool for imaging in neuro-oncology. Many different imaging sequences, allows the representation of various parameters which can, in turn, help to predict tumor characteristics [23]. A histopathology examination is required to definitively determine the tumor type and grade, however, as rapid progress is made in the field of radiomics and artificial intelligence, the prediction of molecular features with the help of MRI is constantly improving [7].

Imaging protocols for investigating brain tumors vary widely among hospitals. However, the US Food and Drug Administration (FDA), the National Cancer Institute (NCI), together with clinical scientists have established a consensus protocol that should be used as a minimum standard for brain tumor studies. This protocol includes precontrast and postcontrast three-dimensional (3D) T1-weighted imaging, axial fluid-attenuated inversion recovery (FLAIR), axial diffusion-weighted imaging (DWI), and axial T2-weighted imaging [24].

T1

Because of excellent anatomical representation, native T1-weighted sequences can be used to accurately describe structural features. However, the more important use case for T1-weighted images is the evaluation of gadolinium contrast enhancement. The contrast agent, which is administered intravenously, shortens T1 relaxation times and enhances tissue contrast in areas where the agent has leaked out of the blood-brain barrier. Since the blood-brain barrier is primarily disrupted in higher-grade gliomas, greater contrast enhancement is typically observed in more aggressive tumors [23].
One feature that could possibly help to predict the glioma subtype is the pattern of contrast enhancement. In a study, conducted by Michiwaki et at., a ring-like contrast-enhancement pattern showed high sensitivity and specificity for glioblastoma, IDH-wild type [25].

Additionally, the pattern of contrast enhancement is associated with the extent of tumor resection and overall survival in anaplastic gliomas. In pre-surgery MRI studies diffuse or ring-like enhancing tumors have been shown to have a significantly lower rate of gross total resection, as investigated by Wang et al. [26].

Another characteristic feature of higher-grade tumors, visible on T1-weighted images is the presence of tumor necrosis. Tumor necrosis appears as a non-enhancing central region within the tumor due to the absence of living cells and blood flow [23].

For a long time, it was believed that higher-grade tumors exhibit necrosis more frequently due to their rapid proliferation, which causes them to outgrow the available blood supply. However, it is now believed that the neoplastic overexpression of pro-coagulants leads to microscopic thrombosis and consequently necrosis. Additionally, necrosis, in turn, alters the tumor's microenvironment, creating conditions that are more favorable for accelerated tumor growth [27].

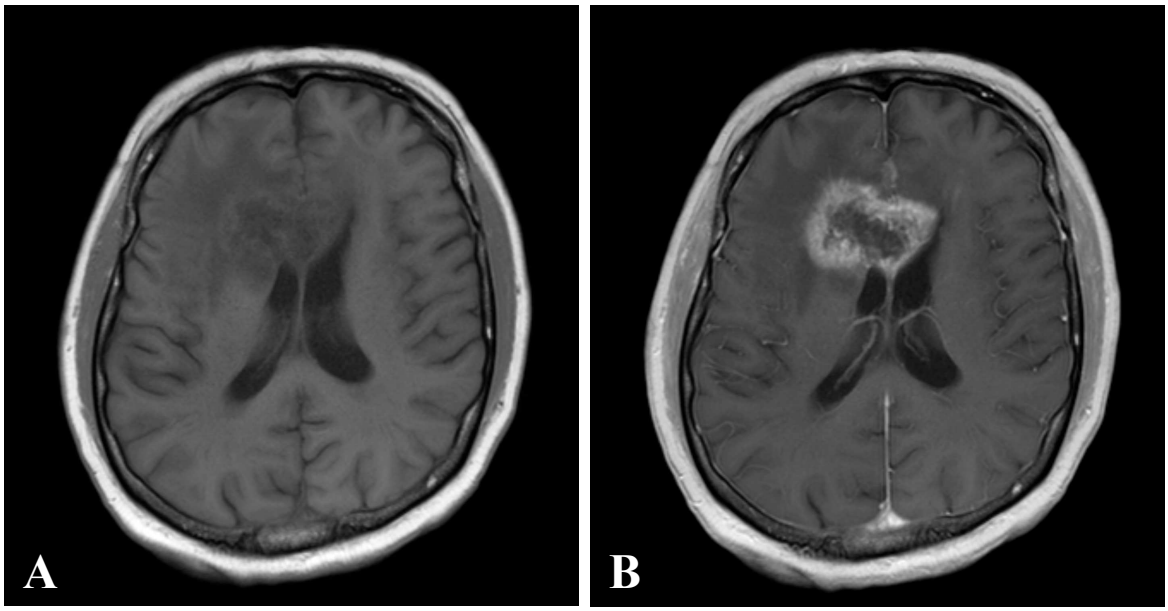

Figure 2: Glioblastoma in T1-weighted MRI sequences. **A** Native axial T1-weighted image showing a hypointense lesion without clear border. **B** Axial T1-weighted image after gadolinium administration, demonstrating ring-like contrast enhancement and central non-enhancing necrosis, typical for higher-grade gliomas.

T2/FLAIR

In T2-weighted images, water and cerebrospinal fluid (CSF) appear bright, while fat in white matter tracts appears darker. When assessing gliomas, T2-weighted images are primarily used to evaluate peritumoral edema, which shows as a hyperintense signal surrounding the tumor core. However, because the strong signal from CSF can impede the assessment of water content changes in tumor regions, FLAIR sequences are used to suppress the CSF signal. In higher-grade gliomas, peritumoral edema often contains spreading tumor cells and is referred to as infiltrative edema. In contrast to vasogenic edema, which is commonly seen in metastases and lower-grade gliomas and which results from fluid leakage caused by a disruption of the blood-brain-barrier (BBB), infiltrative edema can occur without a complete disruption of the BBB. As a result, infiltrative edema can be considered a non-enhancing tumor, reflecting areas where tumor cells are present but do not show enhancement on imaging due to the partially intact blood-brain barrier [28]. Because infiltrative edema reflects tumor spread, the extent of edema could potentially be considered a prognostic factor for overall survival in patients with glioblastoma [29].

Diffusion-Weighted Imaging

DWI is a MRI technique that measures the movement of water molecules within tissue. This movement varies, depending on the cellular environment. In regions with dense cellular structures, like tumors or infarcts, the diffusion of water molecules is more restricted com-

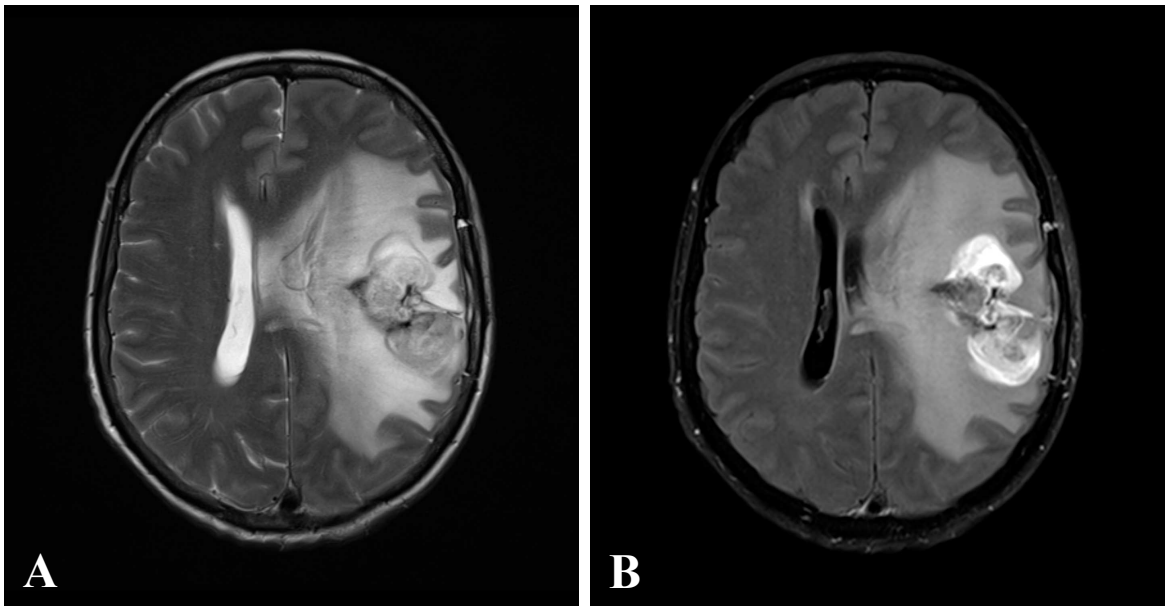

Figure 3: Glioma in T2-weighted MRI sequences. **A** Axial T2-weighted image showing a lesion with surrounding edema. The signal intensity of the cerebrospinal fluid in the ventricles is also high, making it difficult to distinguish edema from CSF. **B** Axial contrast-enhanced FLAIR image showing an enhancing lesion with peritumoral edema. Due to suppression of the CSF signal, the surrounding edema can clearly differentiated from the cerebral ventricles.

pared to healthy tissue. From DWI, the Apparent Diffusion Coefficient (ADC) can be calculated, which quantifies the degree of water diffusion within tissues [30].

In brain tumor diagnosis DWI can help to distinguish necrotic brain tumors from abscesses with greater confidence as abscesses typically show significantly restricted diffusion due to the high viscosity and cellularity of the pus, resulting in very low ADC values. In contrast, necrotic areas within brain tumors usually demonstrate higher ADC values, reflecting the presence of free fluid [31]. Higher-grade gliomas are associated to have lower ADC-values reflecting the increased cellular density in more aggressive tumors. Studies have also shown a poorer prognosis of gliomas with lower ADC-values independent of tumor grade [32]. Some studies suggest that ADC values can be used to evaluate whether peritumoral edema is infiltrative or vasogenic in nature. However, this premise is controversial and has not been confirmed in all studies [33].

1.2.2 Follow-up evaluation

After initial treatment, MRI plays an important role in post-operative assessment and during follow-up controls. The NCCN recommends MRI within 48 to 72 hours after surgery, again 2 to 8 weeks following RT, then every 2 to 4 months for the first 3 years, and subsequently every 3 to 6 months [34].

Post-surgical assessment

After maximal safe resection, which is considered the preferred first line approach for all diffuse gliomas, the primary focus of MRI evaluation is the precise determination of the extent of resection. As shown by García-Ruiz et al., as well as other studies, the extent of resection allows stratification into prognostic groups, as EOR is associated with overall survival and disease progression [35, 36] There is no general recommendation regarding the optimal groups of stratification. While some studies demonstrate a survival advantage using a binary approach (e.g., ≥98% vs. <98% tumor resection), others suggest a precise quantification of the contrast enhancement as there seems to be a continuous association with OS and PFS [35, 37].

Evaluating tumor progression and treatment response

After initial post-surgical assessment, regular follow-up scans are recommended to evaluate treatment response and possible tumor progression. In 2010, the "Response Assessment in Neuro-Oncology" (RANO) criteria were introduced, replacing the previously used Macdonald criteria [38]. Although these criteria incorporate T2/FLAIR to include non-enhancing tumor components, as well as clinical features, the differentiation between true tumor progression and treatment related changes remains challenging. Two events, namely pseudoprogression (PsP) and radiation necrosis (RN) should be discussed in more detail. These two treatment-related changes typically occur at different timepoints following therapy, leading to their classification as early and late post-treatment changes. Pseudoprogression is considered an early change, and is often seen within the first months after RT, while radiation necrosis is typically a late effect, usually developing months to years after treatment [18].

Early post-treatment alterations

Pseudoprogression is radiologically defined as a area of new or enlarged contrast enhancement on follow-up MRI, which subside or stabilize without further treatment and is typically found in the 3 to 6 months after the completion of radiochemotherapy [39]. In malignant gliomas PsP can occur in up to 35% of patients [40]. The pathophysiological mechanisms underlying pseudoprogression are not yet fully understood, it is believed, that increased vessel permeability which leads to increased tumor enhancement occurs as an over-response to therapy [39]. DWI, as well as perfusion weighted imaging (PWI) play a major role in differentiating between true progression and pseudoprogression. On ADC maps, pseudoprogression typically shows elevated ADC values, indicating less restricted diffusion due to vasogenic edema. In TP the relative cerebral blood volume (rCBV), determined by PWI, typically exhibits higher mean and maximum values due to the increased vascularity. Although DWI and PWI act supportive in distinguishing true progression from pseudoprogression, universally

accepted criteria are not yet established [18].

Late post-treatment alterations

Radiation necrosis differs from pseudoprogression in its time of occurrence, as it is typically developing 6 to 12 months after the completion of radiotherapy. In rare cases RN can also occur years after radiation therapy. Pathologically RN is a severe local tissue reaction ultimately leading to necrosis of cerebral blood vessels and brain parenchyma. Radiologically, it presents as a space-occupying lesion, typically associated with neurological symptoms [39]. Similar to pseudoprogression, the differentiation between true progression and RN relies heavily on diffusion-weighted imaging and perfusion-weighted imaging, with RN typically showing lower ADC values and TP demonstrating elevated rCBV values compared to radiation necrosis [18].

1.3 Susceptibility-Weighted Imaging (SWI)

1.3.1 Technical overview

Susceptibility

Magnetic susceptibility, often simply referred to as susceptibility, is a physical property that describes how much a material becomes magnetized when it is placed in an external magnetic field. The magnetization of a material is influenced by various mechanisms, which are primarily related to the atomic structure of the material, especially the behavior of electron orbits and spins. Based on these characteristics, an internal magnetization, also called polarization (J), is generated when an external magnetic field is applied. If the polarization vector aligns with the applied field, the internal magnetic field is reinforced, the magnetic field lines become more concentrated within the object and the magnetic field becomes stronger. This effect is known as paramagnetism, superparamagnetism, or ferromagnetism, depending on the extent of the field enhancement. If the polarization opposes the applied field, the effective internal field is reduced, causing the magnetic field lines to be dispersed or ”pushed out” (Figure 4). As a result, the magnetic field within the material becomes weaker, an effect called diamagnetism. The quantification of this effect can be expressed by the magnetic susceptibility which is denoted as the Greek letter Chi. It is defined as the ratio of the induced magnetization (J) to the applied magnetic field strength (B_0) [41]:

$$\chi = \frac{J}{B_0}$$

Diamagnetic materials exhibit negative susceptibility ($\chi < 0$), while paramagnetic, superparamagnetic, and ferromagnetic materials have positive susceptibility ($\chi > 0$).

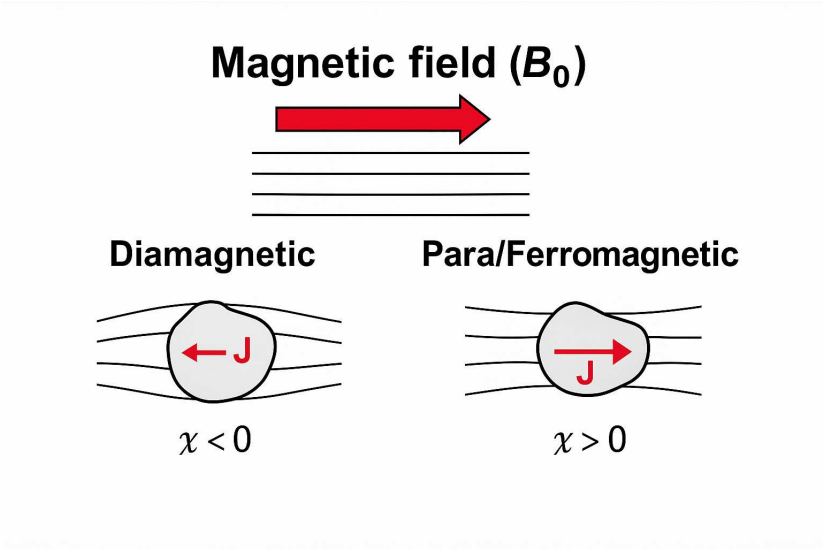

Figure 4: Magnetic field interaction with different materials. Illustration of the behacior of magnetic field lines in diamagnetic and para-/ferromagnetic materials. In diamagnetic materials, the internal polarization (J) opposes the applied field (B_0) causing the field lines to be pushed out. If J points to the same direction an B_0 the magnectic field lines are concentrated. Adapted from Allen D. Elster [42]

In brain tissue, most ions and molecules have electron-orbits that cause magnetic fields opposing the applied field, an effect known as Langevin diamagnetism. However, a few substances show different behavior, such as ferritin, hemosiderin, and deoxyhemoglobin. In these materials the Langevin diamagnetism is exceeded by the spins of unpaired electrons resulting in a paramagnetic effect [43].
This effect is used to generate susceptibility weighted images in MRI which allow the investigation of tissue composition and the presence of iron-rich compounds or blood oxygenation alterations.

Capturing susceptibility effects

When performing MRI, the nuclear spin with its associated magnetic momentum is used to build up a net magnetization (M_0), in the direction of the applied static magnetic field B_0. After excitation with a radiofrequency (RF) pulse (B_1), the net magnetization M_0 is deflected from the established equilibrium state. Due to the now occurring precessional motion of the magnetization in the transverse XY-plane, a signal is generated in the receiver coils. However, due to so-called relaxation effects, a permanently measurable signal is not achieved, but rather a restoration of the equilibrium state. The change in the magnetic field can be described by the Bloch equation (Figure 5) [44]. T1 and T2 are constants that describe the relaxation, where T1 describes longitudinal and T2 transversal relaxation. Gamma (γ) is the gyromagnetic ratio that defines the Larmor frequency - the rate at which nuclear spins precess in the external magnetic field. In MRI, the Larmor frequency determines the resonance condition necessary

for excitation and signal detection.

$$\frac{dM}{dt} = M \times \gamma B - \frac{M_x e_x + M_y e_y}{T_2} - \frac{(M_z - M_0)e_z}{T_1}$$

Figure 5: Bloch equation describing the time-dependent change of the magnetization vector M.

For the transverse relaxation, natural T2-decay, which comes from interactions at the atomic or molecular levels, is always accompanied by additional signal loss caused by magnetic field inhomogeneities. These inhomogeneities, resulting from the varying susceptibility properties of different materials, are the source of contrast in susceptibility-weighted imaging. T2* is used to denote both the tissue-dependent effects of the constant T2 and the effects caused by inhomogeneities in the magnetic field B_0. As relaxation occurs much more rapidly due to these inhomogeneities, susceptibility effects contribute to T2* to a much greater extent than natural T2 effects [45, 46].
Traditionally gradient-echo sequences were used to capture T2* effects. In these sequence a single RF pulse is applied to excite the spins in the tissue. After an initial dephasing gradient, a readout gradient is applied in the opposite direction, which causes the previously dephased spins to rephase, forming an echo. The echo time (TE) is defined as the interval between the application of the RF pulse and the collection of the echo signal. By using longer TE values more dephasing can occur which leads to a stronger T2* signal. However, to archive whole-brain coverage within a reasonable scanning time historically a relatively short echo time was used which led to a less sensitive detection of microbleeds and small susceptibility changes. Modern SWI sequences are based on a three-dimensional gradient-echo-sequence, that allow high spatial resolution, and introduce extensive post-processing methods to enhance image quality. One major improvement is that magnitude and phase information can be displayed independently. In SWI processing involves unwrapping the phase data and applying high-pass filtering to remove background field inhomogeneities. The filtered phase map is then used to create a phase mask, which is combined with the magnitude image to produce the final susceptibility-weighted image. This phase mask enhances areas with susceptibility differences, such as veins and microbleeds, making them appear darker and easier to detect. Modern SWI also uses maximum intensity projection, which enhances the visibility of structures that occur on more than one slice by combining the information of multiple slices into one image [47].

1.3.2 Applications in glioma evaluation

In addition to gadolinium enhanced T1-weighted images, T2/FLAIR images and diffusion weighted images, SWI sequences have become an important component of standard MRI

protocols for tumor evaluation. With the widespread use of modern 3T scanners, the scan time for SWI is now less than 5 minutes, making it easy to include this sequence in the protocol [48].
As SWI is highly effective in distinguishing ferritin, hemosiderin and deoxyhemoglobin from the surrounding brain tissue, its main strength lies in the detection of blood products within the brain tissue. Deoxyhemoglobin is the form of hemoglobin that has released its oxygen and is typically found in acute hemorrhage and in venous blood vessels. Ferritin is a protein that stores iron within cells and can accumulate in regions where chronic microbleeding occurs. Hemosiderin is a breakdown product of hemoglobin and is also often seen in conditions involving chronic or repeated hemorrhages. While SWI can effectively detect these substances, distinguishing between them is not possible, as they all have paramagnetic properties. Calcium, which may also be present in brain tissue can also be detected in SWI, however, due to its diamagnetic behavior, calcium can be distinguished from blood-products using phase maps [47].

ITSS

Intratumoral susceptibility signals (ITSS) are defined as areas of low signal intensity that appear as fine linear or dot-like structures within the tumor on high-resolution SWI [49].
Blood products and calcifications alter the susceptibility signal, however identifying the exact nature of specific ITSS remains challenging. In gliomas, ITSS mainly reflects microbleeds, calcifications, and venous vasculature and as these features are typically absent in other pathologies such as multiple sclerosis, inflammatory granulomas, or lymphomas the evaluation of the susceptibility signal alterations aids in differential diagnosis. Including high-resolution SWI in the MRI protocol increases the specificity for differentiating non-tumorous lesions from high-grade gliomas to 100%. This study by Kim et al. also demonstrated a high prevalence of ITSS, with SWI-signals-alterations present in all glioblastomas examined (n = 25/25) [50].
Beyond differential diagnosis, ITSS serves as a visual biomarker for assessing tumor grade. Pinker et al. demonstrated that high-grade lesions exhibit a high or medium frequency of susceptibility effects (SusE) in 90% of cases, while low-grade lesions show a low frequency or absence of SusE. On histopathological samples, it was shown that intralesional SusE reflect conglomerates of increased tumor microvascularity. This makes sense, as fast-growing tumors, such as high-grade gliomas, rapidly form new, abnormally structured, blood vessels. In addition, these capillaries tend to be wider and have more leaky walls with gaps between the endothelial cells. As a result, these neocapillaries often cause edema in the surrounding tissue and carry a higher risk of bleeding. Both the presence of enlarged capillaries and microbleeds show susceptibility signal alterations on SWI [51].
Park et al. introduced a semiquantitative grading system, based on the visual appearance, to

quantify the extent of ITSS. This system differentiates three primary structures: conglomerated dots, fine linear structures, and a combination of dots with fine linear structures. The degree of ITSS is determined based on the number of these signal alterations within a continuous tumor area: grade 0, no ITSS; grade 1, 1–5; grade 2, 6–10; and grade 3, ≥11. A key finding of the study was the significant correlation between the degree of ITSS and the rCBVmax values within the same tumor segments. This correlation again shows the association between ITSS and increased tumor vascularity, as elevated rCBVmax values are reflecting the increased microvascular density and blood volume [49].

1.3.3 Ring like hypointense SWI signals in neuropathology

Paramagnetic rim lesions in multiple sclerosis

Multiple sclerosis (MS) is a chronic autoimmune disease that affects the CNS, leading to inflammation, demyelination, and neurodegeneration. With the widespread availability of high-quality susceptibility-weighted imaging, two imaging features of multiple sclerosis lesions have gained significance importance. One of them is the central vein sign, which helps to differentiate MS from similar disorders, as the vasocentric origin is typically for an MS lesion [52].
The second feature, currently a focus of extensive research, is the paramagnetic rim lesion (PRL), also referred to as iron-rim lesion. PRLs appear as an hyperintense MS lesion on T_2-weighted imaging, characterized by an hypointense, ring-like signal on SWI, that co-localizes with the outer edge of the lesion [53]. They were first described in 7 Tesla-MRI-studies, however, follow up studies also proved it´s presence and a similar detection rate on 3 Tesla MRI [50, 54]. The presence of PRL is associated with more severe disease progression and is currently being investigated as an important imaging biomarker [50].
Although the histopathological mechanisms behind the formation of the ring-like hypointense signal are not yet fully understood, it is believed that iron metabolism in microglia and astrocytes plays a crucial role. In the CNS, microglia exist in a non-polarized M0 state, a proinflammatory M1 phenotype, or an anti-inflammatory, phagocytic M2 phenotype. Exposure to iron has been shown to induce a shift from the M2 to the M1 state, thereby leading to proinflammatory behavior. In MS oligodendrocyte death due to demyelination in multiple sclerosis leads to an extensive release of iron, which is believed to create a vicious cycle of neuroinflammation. The paramagnetic rim on SWI possibly represents the these iron laden microglia in chronic active MS lesions [52].

The hypointense rim sign in brain abscesses

Brain abscesses are another neuropathology in which a ring-like hypointense signal on SWI has been reported. One study by Toh et al. reported that the presence of a dual rim sign on

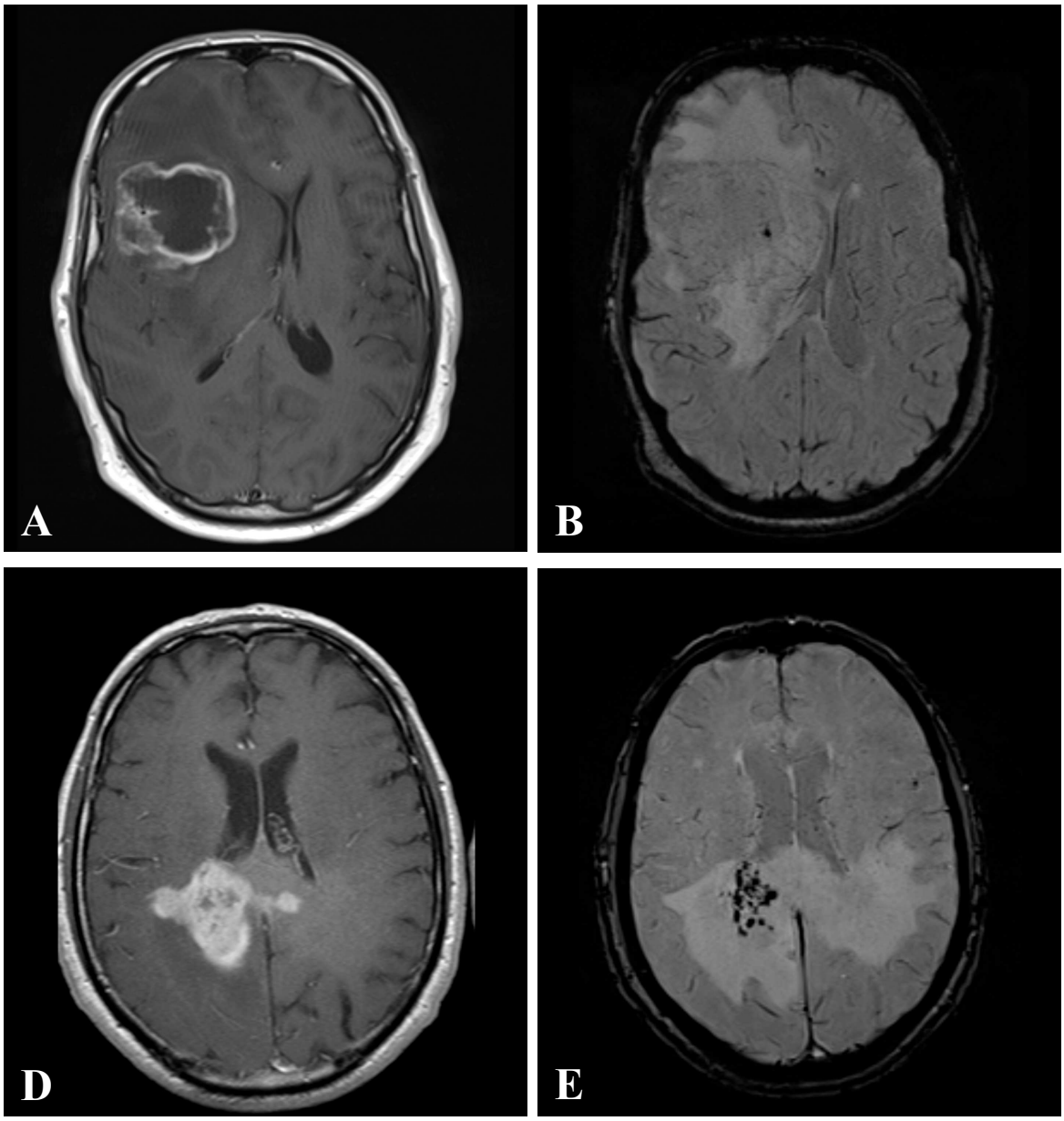

Figure 6: Examples ITSS in two glioma patients. **A–B** Axial contrast-enhanced T1-weighted (A) and corresponding SWI (B) images from a patient with a glioma showing ring-like enhancement and minimal ITSS (grade 1). **D–E** Axial contrast-enhanced T1-weighted (D) and SWI (E) images from a different patient with a large, irregularly enhancing glioma and extensive ITSS (grade 4), visible as multiple dark signal foci, suggesting pronounced intratumoral microhemorrhage.

SWI can help to differentiate pyogenic brain abscesses from glioblastoma, as this imaging feature likely represent paramagnetic free radicals in the abscess capsule. There was also a higher presence of rims described as "smooth" and "complete" in abscesses compared to glioblastomas. The authors speculate that in glioblastomas random deposition of blood products at the edge of the necrotic cavity was the cause of an hypointense ring-like signal [55]. Another study by Antulov et al. continued investigating the hypointense rim in brain abscesses and found, that it could help in distinguishing pyogenic from fungal abscesses as the

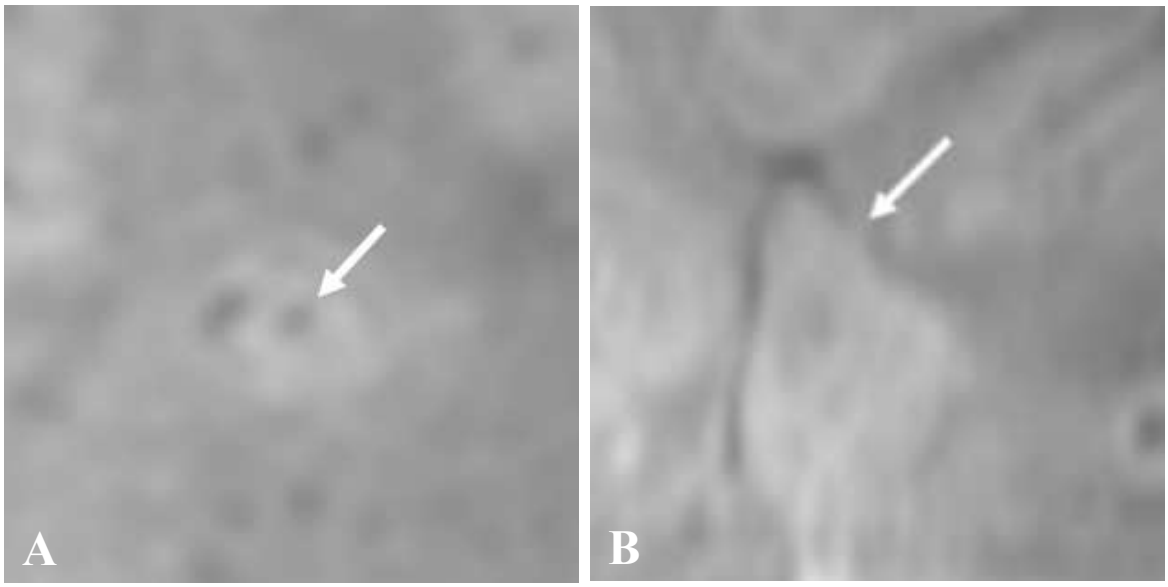

Figure 7: Central Vein Sign and Paramagnetic Rim Lesion. **A** The central vein appears as a dark spot in the center of the lesion on SWI. **B** A chronic active MS lesion with a hypointense rim on SWI, indicating ongoing inflammation and iron accumulation. Adapted from Rimkus et al. (2024) [52].

dual rim sign appears to be specific to pyogenic abscesses [56].

2 Methods

2.1 Aim

As described, SWI has gained significant importance in the assessment of neuropathologies over the last decade. Besides its primary role in the investigation of microbleeds, SWI appears to represent neuropathological features that help to better characterise disease. In MS, a hypointense "iron rim" observed on SWI is thought to represent iron-laden macrophages at the lesion edge and has been associated with worse disease outcomes [55]. In pyogenic brain abscesses, a dual rim sign is observed, allowing better differentiation from necrotic glioblastomas and fungal abscesses [56].

In this study, the role of ring-like hypointense signals on SWI is investigated in the context of treated glioblastoma. This feature may not only represent blood products but also neuroimmunological processes that could influence disease progression and survival. The analysis evaluates the prevalence of hypointense rim signals on SWI, their association with other imaging features, and their effect on overall survival.

Glioblastoma is a highly aggressive disease and treatment response is hard to evaluate. To our knowledge, no studies to this date have investigated the prognostic relevance of SWI features in treated glioblastoma. The present work seeks to identify imaging biomarkers that could potentially provide clinically relevant information on prognosis and treatment and offer a more detailed insight into the underlying pathophysiology.
The following sections describe the methods used to investigate the hypointense rim sign on SWI in patients with glioblastoma. We aimed to assess the association between the hypointense rim and other imaging features, as well as to evaluate its prognostic value for overall survival.

2.2 Study design and ethical approval

This study was designed as a retrospective observational cohort study, approved by the Ethics Comittee of the Hospital University Clinic of Graz (31-423 ex 18/19). The research followed the principles outlined in the Declaration of Helsinki. All patients provided written informed consent before undergoing MRI examinations.

2.3 Study population

We retrospectively identified patients with histologically confirmed, IDH-wildtype glioblastoma who received standard therapy between January 2015 and December 2024 at the Medical University Center Graz, Austria from institutional databases. To be eligible for this

study, patients had to undergo surgical treatment followed by post-surgery radiotherapy. The histopathological diagnosis, available for all patients, was made according to the WHO classification of CNS tumors.

Patients underwent either tumor resection or biopsy only. For resected tumors, we defined total resection as >98% removal of the contrast-enhanced tumor mass and partial resection as 15% to 98% removal. Tumors with <15% removal were categorized as biopsy only. The extent of resection was assessed based on postoperative contrast-enhanced MRI scans, reviewed by a senior neuroradiologist.

2.4 MR imaging protocol

Most MRI scans were acquired on a 3 Tesla MRI scanner. In a few individual cases, a 1.5 Tesla scanner was used due to organizational constraints. Presurgery MRI was obtained up to 3 weeks prior to surgery, while post-radiotherapy MRI scans were obtained within 6 months following the completion of radiation therapy.

For the 3.0 Tesla SIEMENS MAGNETOM Prisma fit scanner (Siemens Healthineers) the protocol included axial T1-weighted sequences (repetition time (TR), 738ms; TE, 8.6ms; flip angle 150°), acquired with a field of view (FOV) of 210 × 210mm and voxel size of 0.8 × 0.8 × 5.0mm. T2-weighted FLAIR images were obtained in axial orientation using a dark-fluid turbo inversion recovery sequence (TR, 8700ms; TE, 81ms; inversion time (TI), 2460ms; flip angle, 150°), with an FOV of 210 × 210mm and voxel size of 0.7 × 0.7 × 5.0mm. Susceptibility-weighted imaging (TR, 28 ms; TE, 20 ms; flip angle, 15°) was performed , with an FOV of 210 × 210mm and an acquisition voxel size of 0.5 × 0.5 × 2.5mm.

For the 1.5 Tesla SIEMENS MAGNETOM (Siemens Healthineers) protocol, axial T1-weighted sequences (TR, 550 ms; TE, 11 ms; flip angle; 70°) were acquired with a FOV of 210 × 210 mm and a voxel size of 0.4 × 0.4 × 5.0 mm. T2-weighted dark-fluid FLAIR images (TR, 8000 ms; TE, 114 ms; TI, 2371 ms; flip angle, 150°) were obtained in axial orientation, using a voxel size of 0.4 × 0.4 × 5.0 mm. Susceptibility-weighted imaging was performed using a 3D gradient-echo sequence (TR, 49 ms; TE, 40 ms; flip angle, 15°) with an acquisition voxel size of 0.8 × 0.8 × 2.5 mm.

All post-contrast sequences were acquired following intravenous injection of gadolinium-based contrast agent (0.1 mmol/kg body weight).

2.5 Image analysis

Each patient had at least one MRI study available, performed within six months after completion of radiation therapy, including the following sequences: T1-weighted imaging (T1-wi), contrast-enhanced T1-wi, FLAIR, and SWI. Patients were excluded if any of these sequences were unavailable.

All available MRI studies performed within the six-month period after radiation therapy were retrieved and reviewed. The first MRI demonstrating a contrast-enhancing mass of ≥10 mm was selected for analysis. If a preoperative MRI, meeting the requirements was available, it was included for analysis.

Patients were excluded from this study if no post-radiotherapy MRI study showed a contrast-

enhancing tumor lesion of at least 10mm.

All images were reviewed by two neuroradiologist with 8 and 15 years of experience. Inter-observer differences were resolved by consensus.

Assessment for the hypointense rim sign

All SWI sequences were evaluated for the presence of a hypointense rim, defined as a linear zone of signal hypointensity situated within, or along the outer boundary of the contrast enhanced tumor. To differentiate the rim from vascular structures, its presence was required on at least three consecutive axial slices. Phase images were reviewed to ensure a paramagnetic origin of the hypointense signal.
If present, the rim was assessed for border morphology, categorized as either irregular or smooth, and completeness, classified into three categories: 0-33%, 34-66% and >66%. Completeness refers to the proportion of the tumor margin that is covered by the hypointense rim on the axial slice with the most extensive rim appearance.

To assess the spatial relationship between the hypointense rim on SWI and the contrast-enhancing tumor, and to confirm its location in the peripheral part of the contrast enhancement, SWI and post-contrast T1-weighted images were co-registered and overlaid using 3D Slicer (version 5.8.1). The overlay was performed in the slice-controller-view by assigning the T1-weighted image as the background and the SWI sequence as the foreground. The appearance of the hypointense rim was enhanced by applying manual intensity thresholding to the SWI data.

Assessment of other imaging properties

Although the primary focus of the study was to assess the hypointense rim on SWI, additional imaging features were evaluated:

Tumor size

Tumor size was assessed by determining the maximum unidimensional diameter of the contrast-enhanced lesion on post-contrast T1-weighted images and the maximum diameter of the solid tumor component on T2-weighted images.

Necrosis

The presence of necrosis was defined as a region, >50% of the tumor mass, that has high signal on T2-weighted images, low signal on T1-weighted images, and an irregular enhancing border on contrast-enhanced images [29, 57].

Edema

Peritumoral edema (PTE) was evaluated on T2-weighted images and categorized as either "major" for edema extending more than 1 cm beyond the tumor margin, or "minor" for edema extending 1 cm or less [29].

Contrast enhancement pattern

We classified contrast-enhancement-patterns into three distinct types. Nodular enhancement was defined as a focal, well-defined area of homogeneous contrast uptake, ring-like enhancement was defined as a rim of contrast uptake surrounding a central non-enhancing core and net-like enhancement was defined as a fine reticulated pattern of contrast uptake within the lesion, with no clear nodular or ring-like structure [26].

ITSS grade

ITSS grade was evaluated according to the semiquantative approach introduced by Parks et al. [49]. The degree of ITSS was divided into four grades based on the number of dot-like or fine linear intratumoral susceptibility signals: grade 0, no ITSS; grade 1, 1–5; grade 2, 6–10; and grade 3, ≥11 signals within the enhancing area of the tumor. The peripheral hypointense rim was not considered part of the ITSS assessment.
For statistical analysis, ITSS was dichotomized into "minor" (grades 0 and 1) and "major" (grades 2 and 3) ITSS.

Imaging feature	Score	Description
Hypointense rim presence	no, yes	A linear zone of signal hypointensityon SWI situated between the tumor parenchyma and the surrounding edema or in the peripheral parts of contrast enhancement.
Hypointense rim contour	irregular, smooth	Defined based on the shape and continuity of the hypointense rim. Smooth rims are continuous and well-defined; irregular rims are discontinuous and appear clustered.
Hypointense rim completeness	<33%, 33–66%, >66%	Proportion of the tumor circumference showing a hypointense rim on the axial slice with the most extensive rim appearance.
Tumor size	mm	The maximum unidimensional diameter of the contrast- enhanced lesion on post-contrast T1-weighted images.
Necrosis	no, yes	Defined as >50% of the tumor volume showing high T2 signal, low T1 signal, and an irregular enhancing border.
Edema	minor, major	Peritumoral T2-hyperintensity graded by distance from the tumor margin: <1 cm (minor), >1 cm (major).
Enhancement pattern	nodular, ring-like, net-like	Defined based on contrast uptake morphology: nodular (focal, homogeneous), ring-like (peripheral rim), or net-like (fine reticulated).
ITSS	minor, major	Graded 0–3 based on the number of intratumoral susceptibility signals (Parks et al.) excluding the peripheral rim. Grades 0–1 were defined as minor, grades 2–3 as major.

Table 1: Classification of MRI features. Overview of imaging characteristics assessed on SWI, T1-weighted, and T2-weighted MRI.

2.6 Statistical analysis

For all statistical analyses, only hypointense rims covering more than 33% of the tumor were considered rim-positive.

The difference in rim presence between the preoperative MRI and the post-radiotherapy MRI was assessed using McNemar´s test in the subset of patients with available preoperative MRI data. This test is used to evaluate differences in proportions in paired data with dichotomous outcomes, in this case, whether there was a significant change in the presence or absence of a hypointense rim between the two timepoints.

To investigate associations between rim presence and other imaging features on post-radiotherapy MRI, Fisher's exact test was applied to dichotomous variables. For variables with more than two categories (extent of resection, contrast enhancement pattern), the Chi-square test was

used.

OS was defined as the time from the date of initial surgery to the date of death or last known follow-up. Patients were censored if they were still alive or lost to follow-up at the time of analysis.

The Cox proportional hazards model was used to analyze associations with OS. The following candidate variables were screened in the univariate Cox models: age (≥ 65 years), gender, MGMT promotor methylation status, tumor necrosis, tumor size (≥ 50mm), extent of edema, contrast enhancement pattern, ITSS score, extent of resection and the presence of a hypointense rim on SWI.

Variables with a p-value < 0.10 in univariate analysis were selected for multivariate analysis. Additionally, clinically relevant factors (age, extent of resection, MGMT methylation status) were included regardless of univariate significance. The proportional hazards assumption was assessed using Schoenfeld residuals. Results are reported as hazard ratios (HR) with 95% confidence intervals (CI) and p-values. Model discrimination was assessed using the concordance index (C-index).

All analyses were conducted using Python (version 3.12.6) and a p-value <0.05 was considered statistically significant.

3 Results

3.1 Cohort characteristics

We identified a total of 78 patients with pathologically confirmed glioblastoma, treated between January 2015 and December 2024. 6 patients without a contrast enhanced tumor of >10mm and 17 patients without a complete MRI study in the first 6 months post-radiotherapy were excluded. 55 patients (age 59.5 ± 10.9 years; 29 males and 26 females) were included in the final analysis. The flowchart of case selection is shown in Figure 8. 19 patients had both pre-surgery and post-radiotherapy MRI scans available for analysis. The mean time-interval from the completion of radiotherapy until the first MRI meeting the criteria was 63.5 days (95% CI 50.2 to 76.7). The mean time interval from the pre-surgery MRI to surgery was 11.5 days (95% CI: 8.9 to 14.1).

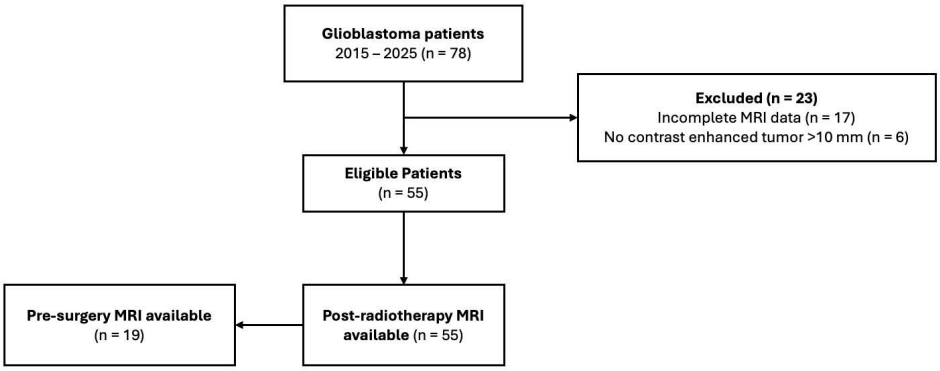

Figure 8: Patient inclusion flow. Flowchart showing the selection of glioblastoma patients diagnosed between 2015 and 2025. Of the 78 patients initially identified, 23 were excluded. A total of 55 patients were eligible for analysis.

MGMT methylation status was available for all patients, with 27 patients (49.1%) showing a promoter methylation, and 28 (50.9%) patients presenting with an unmethylated status. Tumor location was most commonly frontal in 25 out of 55 cases (45.5%), followed by temporal in 17 out of 55 cases (30.9%) and parietal in 12 out of 55 cases (21.8%). Only one patient showed a tumor in the occipital lobe (1.8%). Gross total resection (>97% of the contrast-enhancing tumor removed) was achieved in 17 patients (30.9%), subtotal resection (15–97%) in 19 patients (34.5%), and biopsy-only was also performed in 19 patients (34.5%). Temozolomide was adminisered in 52 out of 55 patients (94.6%).

3.2 Imaging analysis of the hypointense rim sign

We assessed 19 pre-surgery and 55 post-radiotherapy MRIs for the presence of a hypointense rim on SWI. We found a hypointense rim to be present in 7 out of 19 pre-surgery MRIs (36.8%) and 37 out of 55 post-radiotherapy MRIs (67.3%) (Table 2).

Variables	Pre-Surgery	Post-Radiotherapy
Total	19	55
Prevalence	7 (36.8%)	37 (67.3%)
Completeness		
0–33%	1 (14.3%)	3 (8.1%)
34–66%	4 (57.1%)	14 (37.8%)
≥67%	2 (28.6%)	20 (54.1%)
Contour		
Smooth	1 (14.3%)	36 (97.3%)
Irregular	6 (85.7%)	1 (2.7%)

Table 2: Hypointense rim characteristics on SWI before surgery and after radiotherapy. Rim prevalence, completeness, and contour in glioblastoma patients based on pre-surgical (n = 19) and post-radiotherapy (n = 55) SWI.

On pre-surgery MRIs, the rim was classified as 0–33% complete in 1 of 7 cases (14.3%), 34–66% in 4 of 7 cases (57.1%), and >66% in 2 of 7 cases (28.6%). Among post-radiotherapy MRIs, 3 out of 37 rims were classified as 0–33% complete (8.1%), 14 out of 37 as 34–66% complete (37.8%), and 20 as >66% complete (54.1%).

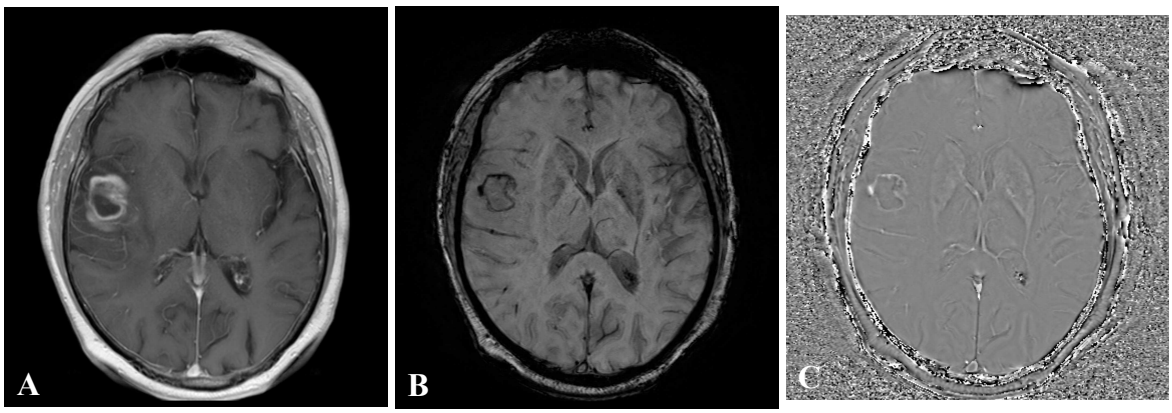

Figure 9: Example of a hypointense rim on SWI in a patient with glioblastoma. **A** Axial contrast-enhanced T1-weighted image showing a ring-enhancing lesion with central necrosis. **B** The corresponding axial SWI image showing a hypointense rim at the tumor margin. **C** Phase image confirming the paramagnetic nature of the rim.

On pre-surgical MRIs, 6 out of 7 rims (85.7%) were classified as irregular, and only 1 rim as smooth (14.3%). For post-radiotherapy MRIs, smooth rims were more frequently observed in 36 out of 37 cases (97.3%), whereas only one irregular rim was present (2.7%).

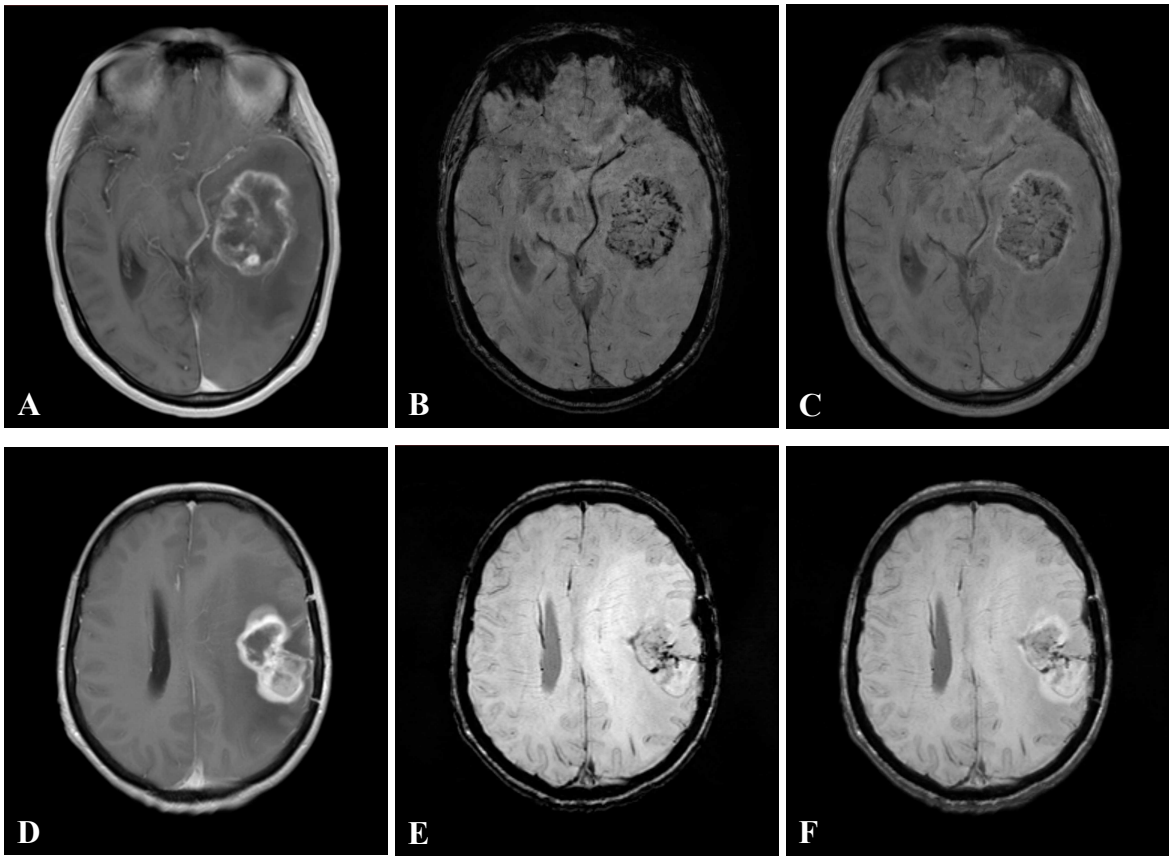

Figure 10: Rim morphology and location in two glioblastoma patients. **A–C** Axial contrast-enhanced T1-weighted (A) and corresponding SWI (B) from a patient with glioblastoma. The fused image (C) shows, that the irregular hypointense rim is located inner to the enhancing margin. **D-F** Another patient with a ring enhancing tumor on contrast-enhanced T1-weighted imaging (D) and a smooth hypointense rim on SWI (E). In the fused image (F), the rim is clearly visible in the posterior portion of the tumor, despite the absence of central necrosis.

We analyzed correlations between the presence of a hypointense rim and clinical as well as radiological features on post-radiotherapy MRIs (Table 3). Due to the small sample size of irregular rims (n = 1), only smooth rims were considered for further analyses. Only rims with a completeness greater than 33% were classified as rim-present.

A statistically significant association was found between the presence of a hypointense rim and the enhancement pattern ($p = 0.004$, Chi-square test), where no rim was observed in tumors with a net-like enhancement ($p = 0.003$, Fisher's exact test). No significant correlation was found between the presence of a hypointense rim and gender, age, MGMT status, necrosis, tumor size, extent of edema, ITSS grade, and extent of resection.

Variables	Number of cases	Hypointense Rim [1]		p-value [2]
		presence	absence	
Total	55	33	22	
Gender				1.000
Male	29	17	12	
Female	26	16	10	
Age				0.125
≥65	14	11	3	
<65	41	22	19	
MGMT				1.000
Methylated	27	16	11	
Unmethylated	28	17	11	
Necrosis				0.512
Yes	43	27	16	
No	12	6	6	
Tumor size				0.495
≥50 mm	11	8	3	
<50 mm	44	25	19	
Edema extent				0.361
Major	41	23	18	
Minor	14	10	4	
Enhancement pattern				**0.004***
Nodular	7	6	1	0.223
Ring-like	42	27	15	0.334
Net-like	6	0	6	**0.003***
ITSS				0.595
Major	30	19	11	
Minor	25	14	11	
Resection extent				0.940
Biopsy	19	12	7	0.779
Partial resection	19	11	8	1.000
Total resection	17	10	7	1.000

[1] Defined as smooth rim with completeness > 33%.
[2] p-values were calculated using Fisher's exact test for binary variables and the Chi-square test was used for variables with more than two categories.

Table 3: Association of clinical and imaging features with the presence of a hypointense rim.

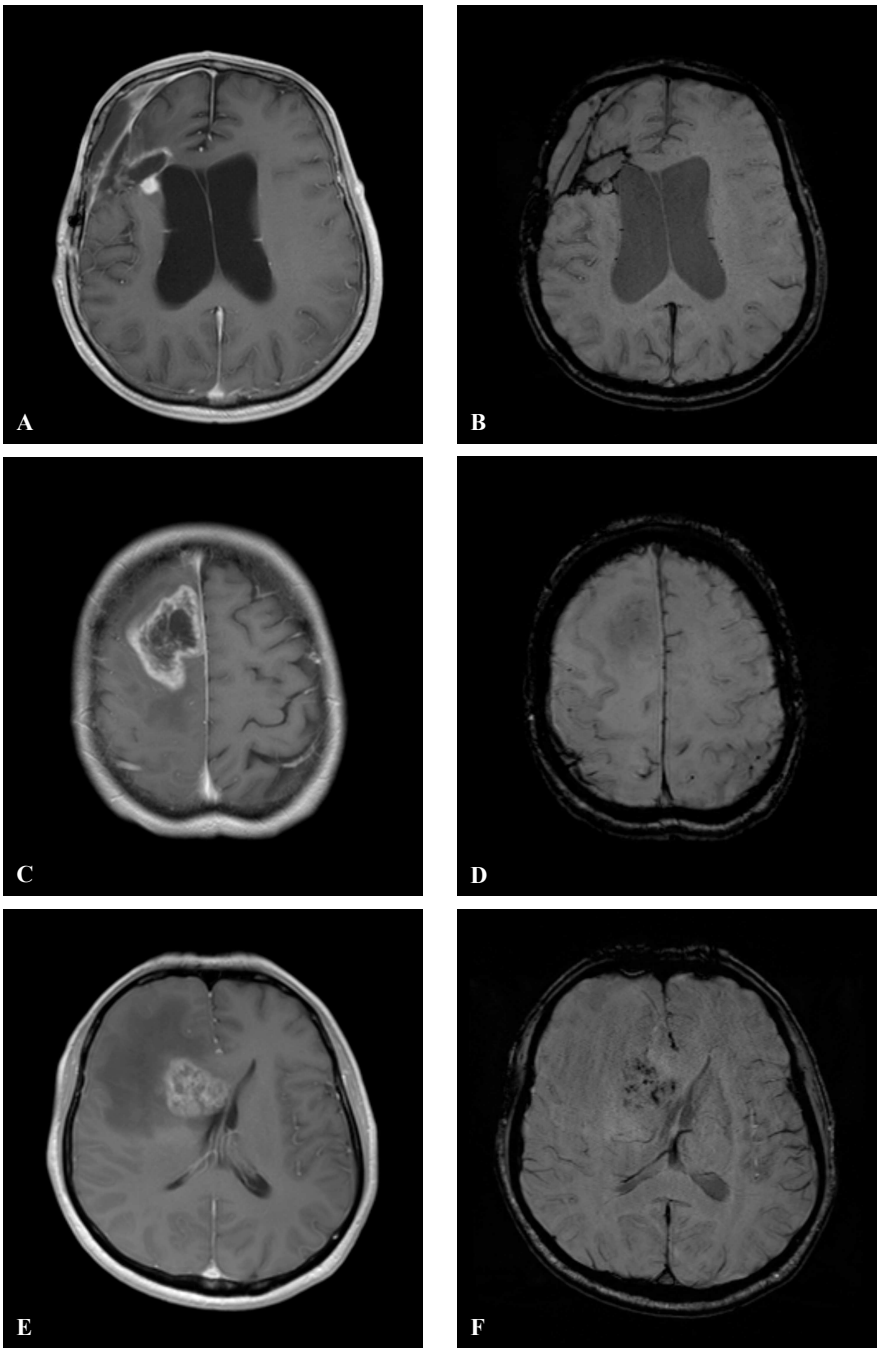

Figure 11: Examples of contrast enhancement patterns and corresponding SWI findings. **A-B** Axial contrast-enhanced T1-weighted image (A) and corresponding SWI (B) showing nodular enhancement next to a resection cavity, with a clearly visible hypointense rim around the nodular enhancement. Note, that the hypointense signal around the resection cavity was not counted as rim, as the enhancement is likely non-tumoral marginal enhancement in reaction to surgival intervention [18]. C-D Ring-like contrast enhancement (C) without a clear rim on the corresponding SWI (D). **E-F** Net-like enhancement pattern (E) with extensive intratumoral susceptibility signals (F), but no hypointense rim.

3.3 Paired subanalysis of the hypointense rim in patients with pre- and post-radiotherapy MRI

To evaluate changes in hypointense rim prevalence before surgery and after radiotherapy, a paired subanalysis was performed in the 25 patients with both pre- and post-treatment MRI

scans. Only rims with a completeness greater than 33% were considered present.

Variables	Pre-Surgery	Post-Radiotherapy	p-value[2]
Total	19	19	
Smooth Rim[1]			**0.003***
No	18 (94.7%)	7 (36.8%)	
Yes	1 (5.3%)	12 (63.2%)	
Irregular Rim[1]			0.221
No	13 (68.4%)	14 (73.7%)	
Yes	6 (31.6%)	5 (26.3%)	

[1] Defined as rim presence with completeness >33%.

[2] McNemar's test. *Statistically significant ($p < 0.05$).

Table 4: Hypointense rim subtype presence before surgery and after radiotherapy in paired patients (n = 19).

A smooth rim was present in 1/19 (5.3%) of pre-surgical MRIs and in 12/19 (63.2%) of post-radiotherapy MRIs, showing a statistically significant increase ($p = 0.003$, McNemar's test). Irregular rims were observed in 6/19 (31.6%) of pre-surgical scans and in 5/19 (26.3%) of post-radiotherapy scans, without a significant difference ($p = 0.221$, McNemar's test).

3.4 Univariate survival analysis

Variable	Hazard ratio (HR)	95% CI	p-value
Gender	0.90	0.50–1.59	0.705
Age	1.49	0.79–2.83	0.222
MGMT	0.59	0.33–1.05	0.074
Necrosis	0.56	0.28–1.13	0.104
Size	1.29	0.65–2.54	0.463
Edema	0.63	0.33–1.20	0.156
Enhancement pattern	1.36	0.66–2.82	0.406
ITSS	0.77	0.44–1.37	0.378
Resection type	1.03	0.73–1.46	0.847
Smooth Rim[1]	**0.47**	**0.26–0.88**	**0.018***

[1] Defined as rim with completeness >33%.

Table 5: Univariate Cox regression analysis.

At the time of analysis (June 2025), 6 out of 55 patients were still alive (10.9%), with a median follow-up of 378 days for all included patients. The median overall survival for the entire cohort was 423 days (95% CI 338 to 524). A univariate survival analysis was performed to assess the association of clinical and imaging features with overall survival. Hazard ratios with 95% confidence intervals and corresponding p-values are presented in Table 5.

Among all variables analyzed in the univariate Cox regression analysis, the presence of a smooth hypointense rim was the only imaging feature significantly associated with overall survival (HR = 0.47, 95% CI 0.26 to 0.88, p = 0.018). Patients with a smooth rim had a 53% lower hazard of death compared to those without. No significant association with overall survival was observed for gender, age, necrosis, tumor size, edema, enhancement pattern, ITSS score, or extent of resection. Patients with MGMT promoter methylation showed a trend toward improved overall survival, almost reaching statistical significance (HR = 0.59, 95% CI 0.33–1.05, p = 0.074).
Kaplan–Meier analysis was additionally performed to visualize overall survival differences based on the presence of a smooth rim (Figure 12).

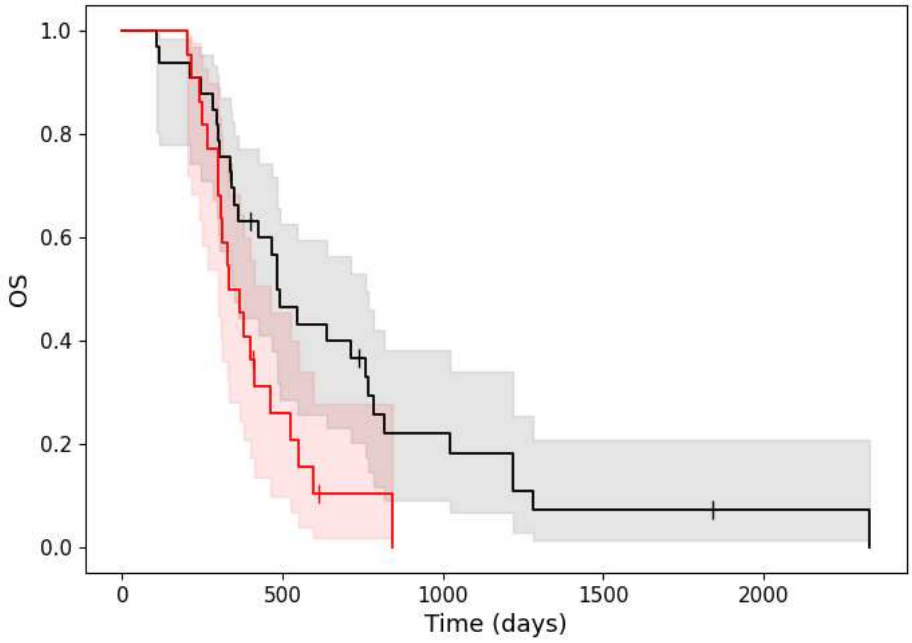

—— **Smooth Rim present** (n = 33):
mOS = 483 days (95% CI: 361 to 761)

—— **Smooth Rim absent** (n = 22):
mOS = 331 days (95% CI: 300 to 410)

p = 0.015

Figure 12: Kaplan–Meier plot of OS for patients with and without a smooth hypointense Rim. 95% confidence interval is shown as shaded area and vertical markers indicate censored patients.

3.5 Multivariate survival analysis

MGMT methylation status and the presence of a smooth hypointense rim were identified as variables associated with survival ($p < 0.10$) in the univariate analysis and were therefore included in the multivariate analysis. Age (≥ 65 years) and extent of resection were included as known prognostic factors in glioblastoma. The Cox proportional hazards assumption was violated for age ($p = 0.0195$) and consequently the model was stratified by this parameter to account for the non-proportionality. The final model included rim presence, MGMT methylation status, and extent of resection as covariates. Hazard ratios with 95% CI and corresponding p-values of this multivariate analysis are presented in Table 6.

Improved overall survival was seen with methylated MGMT promotor (HR = 0.42, 95% CI 0.22 to 0.80, $p = 0.008$) and a smooth hypointense rim (HR = 0.35, 95% CI 0.18 to 0.68, $p = 0.002$). Extent of resection did not show a significant association with survival (HR = 0.93, 95% CI 0.64 to 1.37, $p = 0.727$). The C-index for the multivariate analysis of overall survival was 0.66.

Variables	Hazard ratio (HR)	95% CI	p-value
Resection type	0.93	0.64–1.37	0.727
MGMT Methylation	0.42	0.22–0.80	**0.008***
Smooth Rim[1]	0.35	0.18–0.68	**0.002***

[1] Defined as rim presence with completeness >33%.

Table 6: Multivariate Cox regression model for overall survival. The model was stratified by age.

4 Discussion

In this retrospective study, we analyzed pre-surgery and post-radiotherapy susceptibility-weighted MRI scans, from 55 patients with glioblastoma, to assess the characteristics of a ring-like hypointense signal - referred to as the hypointense rim sign. We examined its morphological features, temporal evolution, associations with other imaging biomarkers as well as influence on overall survival.

Our analysis showed, that the hypointense rim is present in a substantial proportion of patients with glioblastoma in pre-surgery and also post-radiotherapy scans. We observed different levels of completeness and identified two distinct morphological types based on border characteristics: smooth and irregular. This is consistent with observations made by Toh et al., which is to our knowledge the only previous study that assessed a hypointense rim on susceptibility weighted imaging in GBM. Their group reported that 15 out of 20 glioblastomas (75.0%) had hypointense rims on pre-surgery MRI, 13 out of 15 were irregular (87.7%) and 2 out of 15 were smooth (13.3%) [55]. While the overall rim prevalence in our pre-surgical cohort was lower (36.8%), the proportion of smooth rims is consistent with their findings (85.7%). A key difference between the two studies lies in patient selection, as Toh et al. specifically focused on necrotic glioblastomas.

On post-treatment scans, we observed a higher prevalence of hypointense rims (67.3%) compared to pre-surgical scans (36.8%). In a paired subanalysis of the 19 patients with both pre- and post-radiotherapy MRIs, we observed a significant ($p = 0.003$) increase in the prevalence of a smooth hypointense rim after treatment. The post-treatment rims tended to be more complete, with 54.1% of lesions showing ≥66% rim involvement, and more frequently exhibited a smooth contour (97.3%) than an irregular one (2.7%). These findings suggest that the hypointense rim is not simply a static feature that is either present or absent but is changing over time, possibly influenced by both tumor biology and treatment-related effects.

An analysis of the association between smooth rim presence and other imaging features revealed a significant correlation between enhancement pattern and the presence of the hypointense rim. Notably, no rim was observed in any of the cases with net-like enhancement pattern ($p = 0.003$). Although the group size for this pattern was small ($n = 6$), these results suggest that the diffuse infiltrating growth without compact tumor margins is less favorable for rim formation. One possible explanation might be that tumors with net-like enhancement typically lack continuous areas of necrosis. However, this argument is not supported by our data, as we found no significant association between the presence of necrosis and a smooth hypointense rim on post-radiotherapy scans ($p = 0.512$). In our cohort, tumors with clearly defined necrosis frequently lacked a hypointense rim, as shown in Figure 11 A-B, while sev-

eral lesions exhibited a rim despite the absence of necrosis (Figure 11 C-D). Toh et al. had previously speculated that the hypointense rim in glioblastoma, occurs because of random deposition of hemorrhagic products at the edge of the necrotic cavity [55]. However, it is important to note, that they investigated pre-surgery scans and observed a much higher proportion of irregular rims which are more likely to reflect random hemorrhagic depositions. Irregular rims were rare in our cohort of post-radiotherapy scans (n = 1), and no meaningful statistical analysis could be performed for this subgroup.

Overall, our observations suggest that the formation of the smooth hypointense rim cannot be solely explained by the deposition of blood products in a necrotic cavity. However, while no statistically significant association between necrosis and rim presence was observed, we frequently noted that when both were present, the rim often closely mantled the necrotic area, as shown in Figure 10. This spatial relationship indicates a potential biological link between necrosis and rim formation that should be investigated in future studies.

Susceptibility weighted imaging has high sensitivity to detect microhemorrhages and microvessels within glioma, which is typically reflected in the ITSS grade [58]. In our study, we evaluated ITSS grade, based on intratumoral findings, and found no significant correlation between the presence of a hypointense rim and the ITSS grade ($p = 0.595$). Classifying the hypointense rim as part of the ITSS would have led to a methodological bias, as this would create an association between rim presence and ITSS grade. The lack of a significant correlation suggests, that the rim is not just a peripheral extension of intratumoral susceptibility effects but rather a distinct phenomenon with a different underlying pathophysiology. In contrast, we speculate that the irregular rim may reflect clustered microbleeds and may show an association with ITSS in larger cohorts.

Taken together, these findings suggest that the hypointense rim is a dynamic imaging feature that may reflect underlying pathophysiological processes independent of necrosis or intratumoral susceptibility signals. To explore its clinical relevance, we analyzed the association between the presence of a hypointense rim and patient survival.

In our cohort, we identified the smooth rim on SWI as a statistically significant favorable prognostic factor for overall survival in the univariate analysis ($HR = 0.47$, $p = 0.018$). Patients with a smooth rim had a prolonged median survival (16.1 months) compared to those without (11.0 months) as shown by Kaplan–Meier analysis. To our knowledge, this association has not previously been investigated in the context of treated glioblastoma. Notably, none of the other imaging features, showed a statistically significant association with survival in this univariate analysis.

Unexpectedly, there was no significant association (HR = 1.03, p = 0.847) between the extent of resection and overall survival. This finding is not consistent with previous studies reporting that total or near-total resection is associated with prolonged survival [6]. We believe that this can be attributed to our inclusion criteria, which required the presence of a contrast-enhancing tumor measuring more than 10 mm on at least one MRI within the first six months after RT. As a result, patients with a favorable response following resection were excluded, likely leading to an overrepresenation of patients with residual tumor and early disease progression.

Age is another known prognostic factor for glioblastoma that was not associated with survival in our cohort. We speculate that this is because it has been shown that elderly patients do not necessarily benefit from aggressive treatment [59]. As we only included patients who completed surgery followed by concomitant radiotherapy, it is likely that the elderly patients in our cohort represent a subgroup with sufficient performance status to undergo aggressive treatment and thereby the negative prognostic impact of age is not observed.

MGMT promoter methylation was confirmed as an independent predictor of improved survival in the final multivariate model (HR = 0.42, p = 0.008). This is in line with previous studies that demonstrated a better response to alkylating chemotherapy and consecutive improved survival [60]. The smooth rim on SWI was also confirmed as an independent prognostic factor in the multivariate model (HR = 0.35, p = 0.002). This suggests that the presence of a smooth rim provides independent prognostic information and, if confirmed in larger cohorts, should be included into future prognostic models.

Studies that explore the influence of SWI features on patient survival, are rare and primarily focus on the quantity of susceptibility signal. Lupo et al. reported a positive correlation between a higher percentage of hypointensities on SWI within the tumor on pre-surgery MRI and increased progression-free and overall survival. Several studies have shown that highly vascularized gliomas respond better to antiangiogenic drugs, and the group speculated that ITSS quantity can be used to represent abnormal vascularization within the tumor [61, 62]. Following this, one could hypothesize that the hypointense rim at the lesion margin represents abnormal veins which might contribute to a better treatment response. However, several observations from our study lead to the assumption that the hypointense rim does not represent abnormal vascularization. First, the rim often exhibits a continuous, band-like morphology without branching, which is unusual for venous structures. Further to be classified as a hypointense rim we required the presence on at least three consecutive slices. Given, that the axial voxel size was 2.5 mm for all scans it is unlikely that the hypointense rim represents tumor vessels.

In multiple sclerosis, lesions that show a hypointense, paramagnetic rim on susceptibility weighted imaging are associated with chronic inflammation, as the rim has been shown to reflect iron laden macrophages in pathological studies [54]. In glioma, the role of tumor associated macrophages (TAMs) is yet not fully understood, however they are believed to play an important role in disease progression. Oversimplified, macrophages can polarize toward either an M1 phenotype, associated with inflammation and iron sequestration, or an M2 phenotype, which is more likely to release iron into the tumor microenvironment [63]. Pathological studies of brain metastases from breast cancer have shown that tumors exhibit a TAM polarization gradient, with increased iron accumulation at the expanding tumor edge [64]. From these findings, we speculate that the presence of a smooth and continuous hypointense rim in glioblastoma may reflect iron-sequestering M1 macrophages at the tumor margin. One study, conducted by Nazem et al., demonstrated that susceptibility weighted imaging can be used to explore TAM phenotype. They used quantified SWI to demonstrate, that the percentage of susceptibility signal in the enhancing region of the tumor is positively correlated with the L-ferritin positivity percentage on histological samples. L-ferritin is predominant in macrophages with long-term iron storage and an M1 phenotype [65].

Interestingly, the presence of an M1-dominant immune milieu has been linked to prolonged survival, and in our cohort, patients showing a hypointense rim showed significantly improved overall survival [66]. Current research is investigating TAMs as a therapeutic target in glioblastoma, and attempts are made to induce a conversion from an immunosuppressive M2 to a pro-inflammatory M1 phenotype [67].

While the hypothesis, that the smooth hypointense rim reflects M1 macrophages is biologically plausible, direct histological validation in glioblastoma is needed. Prospective studies combining SWI with immunohistochemistry targeting iron-handling and macrophage markers are needed to explore this association.

Another possible explanation is, that organized microenvironmental changes, such as iron-laden macrophage accumulation, are more likely to occur in tumors with slower outward expansion. This could not only explain the association with improved survival but also the increased prevalence and completeness of the rim observed on post-radiotherapy scans, where tumor growth should be substantially altered by treatment.

If validated, the hypointense rim could serve as a non-invasive imaging biomarker, offering potential to assess the response to immune based treatment approaches. Further, since low tumor iron is associated with reduced tumor growth, and iron-laden macrophages can form what could be referred to as an “Iron curtain” around the physical borders of the TME, the spatial distribution of susceptibility signal could provide valuable insights into tumor pro-

gression and growth [64].

4.1 Limitations

This study has several limitations. First, a broad timeframe of 6 months (i.e., 180 days) for the MRI study after completion of radiation therapy was chosen, which could lead to variability in tumor appearance. However, an analysis of the distribution of imaging timepoints showed, that the mean interval between radiation therapy and the selected post-radiation MRI was 63.5 days, with a 95% confidence interval of 50.2 to 76.7 days, indicating that most MRIs were performed within approximately two months after treatment.

Patients who did not have a post-radiation MRI showing a measurable contrast-enhancing tumor within the 6-month timeframe were excluded from the analysis. This applied to patients with disease progression beyond this period, as well as those with rapid progression who did not receive radiotherapy due to poor overall condition. These exclusion criteria may introduce selection bias, potentially limiting the relevance of our findings for the overall glioblastoma population, however, they also provide a well-defined subgroup with measurable disease, allowing a consistent analysis.

One major limitation of the subgroup analysis of patients with pre-surgery and post-radiotherapy MRI is that the enhancing lesion that was evaluated on the post-treatment scan possibly not represents the same tumor tissue that was present before surgery. In many cases, the contrast-enhancing mass may have been partially or completely resected. As a result, a direct comparison of rim characteristics before and after therapy must be interpreted with caution, as they do not necessarily reflect changes within the same anatomical lesion, however it is likely that the residual or recurrent tumor shares similar pathological properties with the original lesion.

Another significant limitation of our study is that interobserver variability was not evaluated. Although two experienced neuroradiologists (8 years and 15 years of experience) resolved discrepancies by consensus, the assessment of imaging features such as rim presence, border morphology and others remains subjective and could introduce bias. For future analysis, it will be important to evaluate interobserver variability using Cohen's Kappa statistic to ensure consistency among different observers.

Although imaging parameters were kept consistent, the use of multiple scanners may have introduced differences in image quality and therefore biased the detection of the hypointense rim and other imaging features.

Finally, this study was conducted using retrospective data from a single-center institution,

which may introduce bias due to patient selection. Further, the number of glioblastoma patients was limited, and the sample size of available MRI studies was small.

4.2 Future outlook

Our study successfully showed, that the hypointense rim sign on SWI is a dynamic imaging feature in a large proportion of glioblastoma patients, and we speculate that it could potentially reflect pathophysiological processes in the tumor-microenvironment. In our cohort, we were able to demonstrate that the presence of a hypointense rim is associated with improved overall survival, indicating its potential value as a prognostic imaging biomarker.

Despite these findings, deeper investigation is needed to confirm our results in larger and independent cohorts. As demonstrated, the hypointense rim is a dynamic feature and standardized time points for post-therapy MRI studies should be established to ensure reliability. Further, to evaluate temporal development, multiple post-radiotherapy scans at defined intervals should be analyzed.
A more detailed assessment of temporal changes would also improve the detection of pseudoprogression, which plays a critical role in the clinical management of glioblastoma patients. Differentiating pseudoprogression from true tumor progression on post-radiotherapy MRI remains a major diagnostic challenge. In addition to DWI and PWI, susceptibility-weighted imaging (SWI) may offer valuable information to help distinguish treatment-related effects from actual tumor growth.

Most importantly, the histological correlate of the hypointense rim sign needs to be evaluated. While pathological studies have been conducted for ITSS, to our knowledge, no studies have investigated the histopathology of peripheral susceptibility signals in detail. In multiple sclerosis, the paramagnetic rim sign has shown to be the result of iron-laden macrophages and demyelination [52]. Its great diagnostic value is now widely recognized and well studied, and we hope that the hypointense rim sign in glioblastoma also holds potential to be established as a radiological marker, once the underlying pathophysiology is better understood.

References

[1] Davis ME. Epidemiology and Overview of Gliomas. Seminars in Oncology Nursing. 2018;34(5):420-9. Available from: https://doi.org/10.1016/j.soncn.2018.10.001.

[2] Louis DN, et al. The 2021 WHO Classification of Tumors of the Central Nervous System: a summary. Neuro-Oncology. 2021;23(8):1231-51. Available from: https://doi.org/10.1093/neuonc/noab106.

[3] Alzial G, et al. Wild-type isocitrate dehydrogenase under the spotlight in glioblastoma. Oncogene. 2022;41(5):613–21.

[4] McNamara C, Mankad K, Thust S, Dixon L, Limback-Stanic C, D'Arco F, et al. 2021 WHO classification of tumours of the central nervous system: a review for the neuroradiologist. Neuroradiology. 2022 Oct;64(10):1919-50. Available from: https://doi.org/10.1007/s00234-022-03008-6.

[5] WHO Classification of Tumours Editorial Board. Central Nervous System Tumours. 5th ed. WHO Classification of Tumours. International Agency for Research on Cancer; 2021.

[6] Brown NF, Ottaviani D, Tazare J, Gregson J, Kitchen N, Brandner S, et al. Survival Outcomes and Prognostic Factors in Glioblastoma. Cancers. 2022 Jun;14(13):3161. Available from: https://www.ncbi.nlm.nih.gov/pmc/articles/PMC9265012/.

[7] Vagvala S, Guenette JP, Jaimes C, Huang RY. Imaging diagnosis and treatment selection for brain tumors in the era of molecular therapeutics. Cancer Imaging. 2022 Apr;22(1):19.

[8] Mitchell D, Shireman JM, Dey M. Surgical Neuro-Oncology: Management of Glioma. Neurologic Clinics. 2022 May;40(2):437-53.

[9] Roth P, Happold C, Weller M. Corticosteroid use in neuro-oncology: an update. Neuro-Oncology Practice. 2015 March;2(1):6-12.

[10] Loghin M, Levin VA. Headache Related to Brain Tumors. Current Treatment Options in Neurology. 2006 Feb;8(1):21-32.

[11] Dang L, White DW, Gross S, Bennett BD, Bittinger MA, Driggers EM, et al. Cancer-Associated IDH1 Mutations Produce 2-Hydroxyglutarate;462(7274):739-44. Available from: https://www.nature.com/articles/nature08617.

[12] Mortazavi A, Fayed I, Bachani M, Dowdy T, Jahanipour J, Khan A, et al. IDH-mutated Gliomas Promote Epileptogenesis through d-2-Hydroxyglutarate-Dependent mTOR Hyperactivation. Neuro-Oncology. 2022 Sep;24(9):1423-35.

[13] Fisher RS, van Emde Boas W, Blume W, Elger C, Genton P, Lee P, et al. Epileptic seizures and epilepsy: definitions proposed by the International League Against Epilepsy (ILAE) and the International Bureau for Epilepsy (IBE). Epilepsia. 2005 Apr;46(4):470-2.

[14] Rudà R, Bello L, Duffau H, Soffietti R. Seizures in Low-Grade Gliomas: Natural History, Pathogenesis, and Outcome after Treatments. Neuro-Oncology. 2012 Sep;14 Suppl 4(Suppl 4):iv55-64.

[15] Parsons MW, Dietrich J. Assessment and Management of Cognitive Symptoms in Patients With Brain Tumors. American Society of Clinical Oncology Educational Book. 2021 Jun;(41):e90-9.

[16] Alizadeh M, Broomand Lomer N, Azami M, Khalafi M, Shobeiri P, Arab Bafrani M, et al. Radiomics: The New Promise for Differentiating Progression, Recurrence, Pseudoprogression, and Radionecrosis in Glioma and Glioblastoma Multiforme. Cancers. 2023 Jan;15(18):4429.

[17] Weller M, van den Bent M, Preusser M, Le Rhun E, Tonn JC, Minniti G, et al. EANO Guidelines on the Diagnosis and Treatment of Diffuse Gliomas of Adulthood. Nature Reviews Clinical Oncology. 2021 Mar;18(3):170-86.

[18] Martucci M, Russo R, Giordano C, Schiarelli C, D'Apolito G, Tuzza L, et al. Advanced Magnetic Resonance Imaging in the Evaluation of Treated Glioblastoma: A Pictorial Essay. Cancers. 2023 Jul;15(15):3790.

[19] Miller JJ, Gonzalez Castro LN, McBrayer S, Weller M, Cloughesy T, Portnow J, et al. Isocitrate Dehydrogenase (IDH) Mutant Gliomas: A Society for Neuro-Oncology (SNO) Consensus Review on Diagnosis, Management, and Future Directions. Neuro-Oncology. 2022 Oct;25(1):4-25.

[20] Bent MJvd, Tesileanu CMS, Wick W, Sanson M, Brandes AA, Clement PM, et al. Adjuvant and concurrent temozolomide for 1p/19q non-co-deleted anaplastic glioma (CATNON; EORTC study 26053-22054): second interim analysis of a randomised, open-label, phase 3 study. The Lancet Oncology. 2021 Jun;22(6):813-23. Publisher: Elsevier. Available from: https://www.thelancet.com/journals/lanonc/article/PIIS1470-2045(21)00090-5/abstract.

[21] Shi W, Scannell Bryan M, Gilbert MR, Mehta MP, Blumenthal DT, Brown PD, et al. Investigating the Effect of Reirradiation or Systemic Therapy in Patients With Glioblastoma After Tumor Progression: A Secondary Analysis of NRG Oncology/Radiation Therapy Oncology Group Trial 0525. International Journal of Radiation Oncology, Biology, Physics. 2018 Jan;100(1):38-44.

[22] Kreisl TN, Kim L, Moore K, Duic P, Royce C, Stroud I, et al. Phase II Trial of Single-Agent Bevacizumab Followed by Bevacizumab Plus Irinotecan at Tumor Progression in Recurrent Glioblastoma. Journal of Clinical Oncology. 2009 Feb;27(5):740-5.

[23] Jacobs AH, Kracht LW, Gossmann A, Rüger MA, Thomas AV, Thiel A, et al. Imaging in Neurooncology. NeuroRX. 2005 Apr;2(2):333-47.

[24] Ellingson BM, Bendszus M, Boxerman J, Barboriak D, Erickson BJ, Smits M, et al. Consensus Recommendations for a Standardized Brain Tumor Imaging Protocol in Clinical Trials. Neuro-Oncology. 2015 Sep;17(9):1188-98.

[25] Michiwaki Y, Hata N, Mizoguchi M, Hiwatashi A, Kuga D, Hatae R, et al. Relevance of Calcification and Contrast Enhancement Pattern for Molecular Diagnosis and Survival Prediction of Gliomas Based on the 2016 World Health Organization Classification. Clinical Neurology and Neurosurgery. 2019 Dec;187:105556.

[26] Wang Y, Wang K, Wang J, Li S, Ma J, Dai J, et al. Identifying the Association between Contrast Enhancement Pattern, Surgical Resection, and Prognosis in Anaplastic Glioma Patients. Neuroradiology. 2016 Apr;58(4):367-74.

[27] Markwell SM, Ross JL, Olson CL, Brat DJ. Necrotic Reshaping of the Glioma Microenvironment Drives Disease Progression. Acta Neuropathologica. 2022 Mar;143(3):291-310.

[28] Villanueva-Meyer JE, Mabray MC, Cha S. Current Clinical Brain Tumor Imaging. Neurosurgery. 2017 Sep;81(3):397-415.

[29] Wu CX, Lin GS, Lin ZX, Zhang JD, Liu SY, Zhou CF. Peritumoral Edema Shown by MRI Predicts Poor Clinical Outcome in Glioblastoma. World Journal of Surgical Oncology. 2015 Mar;13:97.

[30] Baliyan V, Das CJ, Sharma R, Gupta AK. Diffusion weighted imaging: Technique and applications. World Journal of Radiology. 2016 Sep;8(9):785-98. Available from: https://www.ncbi.nlm.nih.gov/pmc/articles/PMC5039674/.

[31] Schaefer PW, Grant PE, Gonzalez RG. Diffusion-Weighted MR Imaging of the Brain. Radiology. 2000 Nov;217(2):331-45.

[32] Mabray MC, Barajas RF, Cha S. Modern Brain Tumor Imaging. Brain Tumor Research and Treatment. 2015 Apr;3(1):8-23.

[33] Pauleit D, Langen KJ, Floeth F, Hautzel H, Riemenschneider MJ, Reifenberger G, et al. Can the Apparent Diffusion Coefficient Be Used as a Noninvasive Parameter to Distinguish Tumor Tissue from Peritumoral Tissue in Cerebral Gliomas? Journal of Magnetic Resonance Imaging. 2004;20(5):758-64.

[34] Horbinski C, Nabors LB, Portnow J, Baehring J, Bhatia A, Bloch O, et al. NCCN Guidelines® Insights: Central Nervous System Cancers, Version 2.2022: Featured Updates to the NCCN Guidelines. Journal of the National Comprehensive Cancer Network. 2023 Jan;21(1):12-20. Available from: https://jnccn.org/view/journals/jnccn/21/1/article-p12.xml.

[35] Garcia-Ruiz A, Naval-Baudin P, Ligero M, Pons-Escoda A, Bruna J, Plans G, et al. Precise Enhancement Quantification in Post-Operative MRI as an Indicator of Residual Tumor Impact Is Associated with Survival in Patients with Glioblastoma;11(1):695. Available from: https://www.nature.com/articles/s41598-020-79829-3.

[36] Majós C, Cos M, Castañer S, Gil M, Plans G, Lucas A, et al. Early Post-Operative Magnetic Resonance Imaging in Glioblastoma: Correlation among Radiological Findings and Overall Survival in 60 Patients. European Radiology. 2016 Apr;26(4):1048-55.

[37] Lacroix M, Abi-Said D, Fourney DR, Gokaslan ZL, Shi W, DeMonte F, et al. A Multivariate Analysis of 416 Patients with Glioblastoma Multiforme: Prognosis, Extent of Resection, and Survival. Journal of Neurosurgery. 2001 Aug;95(2):190-8.

[38] Wen PY, Macdonald DR, Reardon DA, Cloughesy TF, Sorensen AG, Galanis E, et al. Updated Response Assessment Criteria for High-Grade Gliomas: Response Assessment in Neuro-Oncology Working Group. Journal of Clinical Oncology. 2010 Apr;28(11):1963-72.

[39] Qin D, Yang G, Jing H, Tan Y, Zhao B, Zhang H. Tumor Progression and Treatment-Related Changes: Radiological Diagnosis Challenges for the Evaluation of Post Treated Glioma. Cancers. 2022 Aug;14(15):3771.

[40] Abbasi AW, Westerlaan HE, Holtman GA, Aden KM, Van Laar PJ, Van Der Hoorn A. Incidence of Tumour Progression and Pseudoprogression in High-Grade Gliomas: A Systematic Review and Meta-Analysis. Clinical Neuroradiology. 2018 Sep;28(3):401-11.

[41] Schenck JF. The Role of Magnetic Susceptibility in Magnetic Resonance Imaging: MRI Magnetic Compatibility of the First and Second Kinds. Medical Physics. 1996;23(6):815-50.

[42] Elster AD. MRIQuestions.com; n.d. Courtesy of Allen D. Elster. Accessed: 2025-07-20. Available from: https://mriquestions.com.

[43] Duyn J. MR Susceptibility Imaging. Journal of magnetic resonance (San Diego, Calif : 1997). 2013 Apr;229:198-207.

[44] Nakada T. Clinical application of high and ultra high-field MRI. Brain and Development. 2007 Jul;29(6):325-35. Publisher: Elsevier BV. Available from: https://linkinghub.elsevier.com/retrieve/pii/S0387760406002403.

[45] Jensen EC. Technical Review, Types of Imaging, Part 4—Magnetic Resonance Imaging. The Anatomical Record. 2014;297(6):973-8.

[46] Grover VPB, Tognarelli JM, Crossey MME, Cox IJ, Taylor-Robinson SD, McPhail MJW. Magnetic Resonance Imaging: Principles and Techniques: Lessons for Clinicians. Journal of Clinical and Experimental Hepatology. 2015 Sep;5(3):246-55. Publisher: Elsevier BV. Available from: https://linkinghub.elsevier.com/retrieve/pii/S0973688315004156.

[47] Haller S, Haacke EM, Thurnher MM, Barkhof F. Susceptibility-Weighted Imaging: Technical Essentials and Clinical Neurologic Applications. Radiology. 2021 Apr;299(1):3-26.

[48] Soman S, Holdsworth SJ, Barnes PD, Rosenberg J, Andre JB, Bammer R, et al. Improved T2* Imaging without Increase in Scan Time: SWI Processing of 2D Gradient Echo. AJNR: American Journal of Neuroradiology. 2013 Nov;34(11):2092-7.

[49] Park MJ, Kim HS, Jahng GH, Ryu CW, Park SM, Kim SY. Semiquantitative Assessment of Intratumoral Susceptibility Signals Using Non-Contrast-Enhanced High-Field High-Resolution Susceptibility-Weighted Imaging in Patients with Gliomas: Comparison with MR Perfusion Imaging. AJNR: American Journal of Neuroradiology. 2009 Aug;30(7):1402-8.

[50] Kim S, Lee EK, Song CJ, Sohn E. Iron Rim Lesions as a Specific and Prognostic Biomarker of Multiple Sclerosis: 3T-Based Susceptibility-Weighted Imaging. Diagnostics (Basel, Switzerland). 2023 May;13(11):1866.

[51] Pinker K, Noebauer-Huhmann IM, Stavrou I, Hoeftberger R, Szomolanyi P, Karanikas G, et al. High-Resolution Contrast-Enhanced, Susceptibility-Weighted MR Imaging at 3T in Patients with Brain Tumors: Correlation with Positron-Emission Tomography and Histopathologic Findings. AJNR: American Journal of Neuroradiology. 2007 Aug;28(7):1280-6. Available from: https://www.ncbi.nlm.nih.gov/pmc/articles/PMC7977663/.

[52] Rimkus CdM, Otsuka FS, Nunes DM, Chaim KT, Otaduy MCG. Central Vein Sign and Paramagnetic Rim Lesions: Susceptibility Changes in Brain Tissues and Their Implications for the Study of Multiple Sclerosis Pathology. Diagnostics. 2024 Jun;14(13):1362. Available from: https://www.ncbi.nlm.nih.gov/pmc/articles/PMC11240827/.

[53] Bagnato F, Sati P, Hemond CC, Elliott C, Gauthier SA, Harrison DM, et al. Imaging chronic active lesions in multiple sclerosis: a consensus statement. Brain. 2024 Sep;147(9):2913-33. Available from: https://doi.org/10.1093/brain/awae013.

[54] Absinta M, Sati P, Fechner A, Schindler MK, Nair G, Reich DS. Identification of Chronic Active Multiple Sclerosis Lesions on 3T MRI. American Journal of Neuroradiology. 2018 Jul;39(7):1233-8. Publisher: American Journal of Neuroradiology Section: Adult Brain. Available from: https://www.ajnr.org/content/39/7/1233.

[55] Toh CH, Wei KC, Chang CN, Hsu PW, Wong HF, Ng SH, et al. Differentiation of Pyogenic Brain Abscesses from Necrotic Glioblastomas with Use of Susceptibility-Weighted Imaging. AJNR: American Journal of Neuroradiology. 2012 Sep;33(8):1534-8. Available from: https://www.ncbi.nlm.nih.gov/pmc/articles/PMC7966558/.

[56] Antulov R, Dolic K, Fruehwald-Pallamar J, Miletic D, Thurnher MM. Differentiation of pyogenic and fungal brain abscesses with susceptibility-weighted MR sequences. Neuroradiology. 2014 Nov;56(11):937-45. Available from: http://link.springer.com/10.1007/s00234-014-1411-6.

[57] Pope WB, Sayre J, Perlina A, Villablanca JP, Mischel PS, Cloughesy TF. MR Imaging Correlates of Survival in Patients with High-Grade Gliomas. AJNR: American Journal of Neuroradiology. 2005 Nov;26(10):2466-74. Available from: https://www.ncbi.nlm.nih.gov/pmc/articles/PMC7976216/.

[58] Kong LW, Chen J, Zhao H, Yao K, Fang SY, Wang Z, et al. Intratumoral Susceptibility Signals Reflect Biomarker Status in Gliomas. Scientific Reports. 2019 Nov;9(1):17080. Publisher: Nature Publishing Group. Available from: https://www.nature.com/articles/s41598-019-53629-w.

[59] Brandes AA, Franceschi E, Tosoni A, Benevento F, Scopece L, Mazzocchi V, et al. Temozolomide concomitant and adjuvant to radiotherapy in elderly patients with glioblastoma: Correlation with MGMT promoter methylation status. Cancer. 2009 Aug;115(15):3512-8. Available from: https://acsjournals.onlinelibrary.wiley.com/doi/10.1002/cncr.24406.

[60] Pandith AA, Qasim I, Zahoor W, Shah P, Bhat AR, Sanadhya D, et al. Concordant association validates MGMT methylation and protein expression as favorable prognos-

tic factors in glioma patients on alkylating chemotherapy (Temozolomide). Scientific Reports. 2018 Apr;8(1):6704. Publisher: Nature Publishing Group. Available from: https://www.nature.com/articles/s41598-018-25169-2.

[61] Kong Z, Yan C, Zhu R, Wang J, Wang Y, Wang Y, et al. Imaging biomarkers guided anti-angiogenic therapy for malignant gliomas. NeuroImage Clinical. 2018;20:51-60.

[62] Lupo JM, Essock-Burns E, Molinaro AM, Cha S, Chang SM, Butowski N, et al. Using susceptibility-weighted imaging to determine response to combined anti-angiogenic, cytotoxic, and radiation therapy in patients with glioblastoma multiforme. Neuro-Oncology. 2013 Apr;15(4):480-9. Available from: https://www.ncbi.nlm.nih.gov/pmc/articles/PMC3607266/.

[63] Recalcati S, Locati M, Marini A, Santambrogio P, Zaninotto F, De Pizzol M, et al. Differential regulation of iron homeostasis during human macrophage polarized activation. European Journal of Immunology. 2010;40(3):824-35. _eprint: https://onlinelibrary.wiley.com/doi/pdf/10.1002/eji.200939889. Available from: https://onlinelibrary.wiley.com/doi/abs/10.1002/eji.200939889.

[64] DeRosa A, Leftin A. The Iron Curtain: Macrophages at the Interface of Systemic and Microenvironmental Iron Metabolism and Immune Response in Cancer. Frontiers in Immunology. 2021 Apr;12. Publisher: Frontiers. Available from: https://www.frontiersin.org/journals/immunology/articles/10.3389/fimmu.2021.614294/full.

[65] Nazem A, Guiry SC, Pourfathi M, Ware JB, Anderson H, Iyer SK, et al. MR susceptibility imaging for detection of tumor-associated macrophages in glioblastoma. Journal of Neuro-Oncology. 2022 Feb;156(3):645-53. Available from: https://doi.org/10.1007/s11060-022-03947-3.

[66] Zeiner PS, Preusse C, Blank AE, Zachskorn C, Baumgarten P, Caspary L, et al. MIF Receptor CD74 is Restricted to Microglia/Macrophages, Associated with an M1-Polarized Immune Milieu and Prolonged Patient Survival in Gliomas. Brain Pathology. 2015 Jul;25(4):491-504. Available from: https://onlinelibrary.wiley.com/doi/10.1111/bpa.12194.

[67] Hambardzumyan D, Gutmann DH, Kettenmann H. The role of microglia and macrophages in glioma maintenance and progression. Nature neuroscience. 2016 Jan;19(1):20-7. Available from: https://www.ncbi.nlm.nih.gov/pmc/articles/PMC4876023/.